Journal of South American Earth Sciences 108 (2021) 103170

Contents lists available at ScienceDirect

Journal of South American Earth Sciences

journal homepage: www.elsevier.com/locate/jsames

U–Pb geochronology of the meta-volcanic rocks from Sierra de Calcatapul: Implications for the Middle Triassic syn-rift volcanism and tectonic evolution of northern extra-Andean Patagonia

Pablo D. González [a,b,*], Raúl E. Giacosa [b], Silvia Lagorio [c], Carlos Ballivian Justiniano [d], Ana M. Sato [e], M. Cecilia Cábana [f], Miguel A.S. Basei [g], Alicia Busteros [c], Diego Silva Nieto [c]

[a] Consejo Nacional de Investigaciones Científicas y Técnicas (CONICET), Argentina
[b] Servicio Geológico Minero Argentino, Centro General Roca, Río Negro, SEGEMAR Regional Sur, Independencia 1495, Parque Industrial 1, Gral. Roca, (Río Negro), C. P. 8332, Casilla, Correo, Argentina
[c] Servicio Geológico Minero Argentino (SEGEMAR), Instituto de Geología y Recursos Minerales, Av. General Paz 5445, B 1650 WAB, Buenos Aires, Argentina
[d] CONICET, Instituto de Recursos Minerales (UNLP-CICBA), Calle 64 Esquina 120, 1er Piso, (1900) La Plata, Buenos Aires, Argentina
[e] Centro de Investigaciones Geológicas (UNLP-CONICET), Diagonal 113 N° 275, B 1904 DPK, La Plata, Buenos Aires, Argentina
[f] Universidad Nacional de Río Negro, Instituto de Investigación en Paleobiología y Geología, Geomatics Laboratory, Av. Julio A. Roca 1242, R 8332 EXZ, General Roca, Río Negro, Argentina
[g] Conselho Nacional de Desenvolvimento Científico e Tecnológico (CNPq), Centro de Pesquisas Geocronológicas (CPGeo), Instituto de Geociências, Universidade de São Paulo, Cidade Universitária, Rua Do Lago 562, CEP 05508-080, São Paulo, Brazil

ARTICLE INFO

Keywords:
Zircon ages
Half-graben
Extensional tectonics
Post-Choiyoi magmatism
Patagonia

ABSTRACT

This contribution deals first new ICP-MS U–Pb zircon ages that indicate Middle- and Late Triassic magmatic episode and tectonometamorphic events, respectively, for the central Patagonia region, instead of a Paleozoic history as previously estimated. The Calcatapul Formation consists of a (meta-) volcano-sedimentary syn-rift sequence deposited unconformably, shortly after the extensional Gondwanide orogenic collapse, over a basement composed of Permian granites. Two $^{206}Pb/^{238}U$ ages yielded 245.1 ± 2.8 and 244.8 ± 4.1 Ma to magmatic crystallization of ignimbrites, along with another weighted mean of 226.7 ± 4.4 Ma interpreted as the age of the tectonometamorphic event D_1-M_1 affecting the Calcatapul sequence. U–Pb ages open new insights into the tectonomagmatic evolution of the area because the syn-rift wedge deposited in the Uribe and Yancamil half-grabens under the extensional tectonic regime was then inverted along the basin-bounding faults like the Yancamil fault. Inversion tectonics involved reverse fault-related uplift against a buttress of the rigid granitic block, and under dynamic greenschist-to-amphibolite facies metamorphic conditions, before the Late-Triassic granitic magmatism of the Lipetrén Suite took place. The pre-rift granitic basement represents the southern extension of the main magmatic phase of Choiyoi Province in Patagonia, whereas the Middle Triassic recorded the extensional, post-Choiyoi magmatism. The local, compressive D_1 event punctuated an overall widespread lithospheric extension that leads to Gondwana breakup since the earliest Jurassic times.

1. Introduction

The extensive *Choiyoi Magmatic Province* is the main geological feature along the Late Paleozoic continental margin of southwestern Gondwana, as recorded by several contributions (e.g., Rapela and Llambías, 1985; Kay et al., 1989; Sato et al., 2015, among many others). It consists of intermediate to acidic batholiths and associated volcanic rocks with an extension covering most of the morphostructural regions of central Argentina and Chile and extends towards the south and southeast into the North Patagonian Cordillera, Neuquén Basin, and North Patagonian Massif (Llambías and Sato, 2011).

The Choiyoi magmatism is geologically constrained between the

* Corresponding author. Consejo Nacional de Investigaciones Científicas y Técnicas (CONICET), Servicio Geológico Minero Argentino, Centro General Roca, Río Negro, SEGEMAR Regional Sur, Independencia 1495, Parque Industrial 1, Gral. Roca (Río Negro), C.P.: 8332, Casilla, Correo, Argentina..
E-mail addresses: pdgonzalez@unrn.edu.ar, pablo.diego.gonzalez@gmail.com (P.D. González), rgiacosa@unrn.edu.ar (R.E. Giacosa), silvia.lagorio@segemar.gov.ar (S. Lagorio), carlos_ballivian@hotmail.com (C.B. Justiniano), sato@cig.museo.unlp.edu.ar (A.M. Sato), mccabana@unrn.edu.ar (M.C. Cábana), baseimas@usp.br (M.A.S. Basei), alicia.busteros@segemar.gov.ar (A. Busteros), diego.silvanieto@segemar.gov.ar (D.S. Nieto).

https://doi.org/10.1016/j.jsames.2021.103170
Received 16 July 2020; Received in revised form 8 January 2021; Accepted 11 January 2021
Available online 16 January 2021

Early Permian San Rafael orogenic phase, which causes the folding and thrusting of pre-Early Permian rocks, and the Triassic Huárpica extensional phase (Leanza, 2009; Llambías and Sato, 2011), along with three magmatic stages described as (1) pre-Choiyoi orogenic magmatism (Late Mississippian-Artinskian), (2) Choiyoi magmatism, developed mostly between 286 and 247 Ma, and (3) post-Choiyoi magmatism by Middle to Late Triassic (Sato et al., 2015). Both the volcanic and plutonic emplacements of the Choiyoi magmatism are associated with an extensional regime, with volcanic deposits controlled by normal faults (Heredia et al., 2002; Giambiagi and Martínez, 2008), and ~N–S trending axis of plutons related to the extensional collapse of the Gondwanide orogen (Llambías and Sato, 1995). The post-Choiyoi magmatism is associated with the extensional Huárpica phase (Sato et al., 2015), leading to diachronic and isolated initiation of rift depocenters, lava/pyroclastic flows, and ashfall deposits interlayered in the sedimentary syn-rift sequences.

In northern Patagonia at ~39°S, the Choiyoi Magmatic Province spreads eastward with the expansion of the magmatism to the east and southeast, from Neuquén Basin through North Patagonian Massif up to the coast of Atlantic Ocean, as is also recorded by several contributions (e.g., Llambías and Rapela, 1984; Llambías et al., 1984; Caminos et al., 2001; Varela et al., 2005; Pankhurst et al., 2006; Lema et al., 2008; Luppo et al., 2018; Martínez Dopico et al., 2019; Grégori et al., 2020, among others). Although the outcrops of plutons and associated volcanic rocks are interrupted by the Cenozoic basaltic Somuncura plateau, they delineate a near-continuous NW-SE trending Gondwanide magmatic belt with, at least, two apparent parallel branches following along borders of the plateau to the north and south (Ramos, 2008; Grégori et al., 2020).

In this contribution, we first present two new LA-MC-ICPMS U–Pb ages from a representative volcanic unit coeval with the post-Choiyoi magmatism in southern parts of the North Patagonian Massif (Sierra de Calcatapul area at ~42°S-70°W, Fig. 1), and compare them with the ages from volcanogenic events across the mentioned area. The U–Pb ages reported here open new insights into the origin and tectono-magmatic evolution of the final stages of the Gondwanide magmatic cycle in Patagonia. Additionally, we contribute to regional correlations from the geologic and tectonic perspective of the Choiyoi magmatism along the Gondwana continental margin.

2. Regional geology of the Choiyoi Magmatic Province in northern Patagonia

In the North Patagonian Massif, Late Paleozoic to Triassic outcrops of the igneous rocks coeval with Choiyoi Magmatic Province are abundant, both in the eastern and western regions, first gathered into the "*Gondwanide Eruptive Cycle*" by Llambías et al. (1984). The compressive effects of the San Rafael orogenic phase are brittle-to-ductile structures observables in a wide area, affecting the Early Paleozoic igneous-metamorphic basements, as well as middle to late Paleozoic sedimentary and igneous units (Basei et al., 2002; von Gosen, 2002; 2003; 2009; Giacosa, 1997; Greco et al., 2015; González et al., 2018). This situation makes difficult to constrain geologically both the base and the top stratigraphic features of the Choiyoi magmatism on a structural basis. Although the entire magmatic Choiyoi interval is represented in northern Patagonia, they include deformed and undeformed granitoids, even with deformed and metamorphosed volcanic equivalents. Likewise, the ductile deformation and high-grade metamorphism related to the San Rafael phase, in addition to its possible diachrony, are not yet entirely clear in most of the regions (Llambías et al., 2002). For instance, in the western parts of the North Patagonian Massif towards the North Patagonian Cordillera, foliated and non-foliated granitoid plutons range mostly between 330 and 250 Ma time interval (Varela et al., 2005; Pankhurst et al., 2006; Grégori et al., 2020), as well as undeformed and deformed representative volcanic equivalents of them, are broadly coeval, covering the youngest Choiyoi interval between 257 and 246 Ma (Pankhurst et al., 2006; Luppo et al., 2018). Moreover, within the eastern North Patagonian Massif, foliated granitoids and orthogneisses have provided ages as young as 261, 251, and 245 Ma (Varela et al., 2005, 2008; Pankhurst et al., 2006, 2014; Chernicoff et al., 2013; García et al., 2014; Martínez Dopico et al., 2017a), not yet fully understood the relationship between the crystallization ages with deformation of San Rafael phase, and even the effusion of the contemporary volcanic cover, which in turn is also fragilely deformed (Caminos et al., 2001; von Gosen, 2003).

Although equivalent outcrops of the Choiyoi magmatism exist in southern parts of the North Patagonian Massif, they lack U–Pb ages. Therefore, the (meta-) volcano-sedimentary sequence of the Calcatapul Formation, which is the object of study in this contribution, was broadly considered as forming part of the oldest igneous-metamorphic basement. However, they turned out to be younger than expected.

3. Geological outline of the Sierra de Calcatapul and surroundings

In the Sierra de Calcatapul area, the Cushamen Formation is exposed as strips and xenoliths of basement rocks included within younger intrusive plutons (Fig. 1). Its schists, paragneisses, amphibolites, and migmatites have been interpreted as Precambrian-Early Paleozoic (Proserpio, 1978; Volkheimer and Lage, 1981), though Hervé et al. (2005, 2018) provided U–Pb detrital zircon maximum sedimentation ages of 385 and 335 Ma (Givetian-Middle Mississippian), for at least parts of the Cushamen Formation.

According to Proserpio (1978) and Nullo (1978), the Calcatapul Formation (Volkheimer, 1965) is mostly composed of intermediate-to-acidic, effusive and explosive (meta-) volcanic rocks, also containing intercalations of phyllites and meta-conglomerate lenses (von Gosen and Loske, 2014). Its polyphase deformed, low-grade metamorphic rocks have been considered Early-Middle Paleozoic (Proserpio, 1978; Nullo, 1978). Its relationship with the protoliths of the Cushamen Formation is unclear.

The Mamil Choique Formation (Ravazzoli and Sesana, 1977) consists of deformed and undeformed granitoids intruded into the Cushamen Formation. Although they have been assigned to a wide span between the Precambrian and Late Paleozoic, TIMS and SHRIMP U–Pb zircon ages constrain its magmatic crystallization to Early Permian (Varela et al., 2005; Pankhurst et al., 2006; Lagorio et al., 2020). The Yancamil Granite (TIMS U–Pb zircon ages scatter between 263 and 280 Ma, von Gosen and Loske, 2014) and the Laguna del Toro Granodiorite (SHRIMP U–Pb zircon age of 294 ± 3 Ma, Pankhurst et al., 2006) are considered in conjunction with the Mamil Choique Formation as the Late Paleozoic Gondwanide Eruptive Cycle of the North Patagonian Massif. The igneous stratigraphy of the Mamil Choique granitoids has recently been revised and updated in terms of the modern paradigm for the igneous rocks (e.g., Murphy and Salvador, 2002), and then some old terminology has been replaced (e.g., Mamil Choique Granitoids or Batholith, Lagorio et al., 2020; González and Giacosa, 2020).

The leucogranites, porphyritic granites, porphyries, and aplo-pegmatites of the earlier called Lipetrén Formation have been assigned to the Permian (Nullo, 1978; Proserpio, 1978) or Permo-Triassic (Cucchi, 1993). In the sierras de Lipetrén and Calcatapul, the unit intruded the Cushamen-Mamil Choique pair and the Calcatapul Formation, respectively, leading to contact metamorphism (Nullo, 1978; González et al., 1999). In the Gastre area, the granitoids of Lipetrén Formation have been collectively re-named the Lipetrén Suite (or Superunit) and separated from quartz diorites, granodiorites, and monzogranites of the Gastre Suite (or Superunit) by Rapela et al. (1991; 1992). The Horqueta Granodiorite should be considered as belonging to the Gastre Suite (Lagorio et al., 2015; see also Lagorio et al., 2020). Although the Lipetrén and Gastre suites have been included as part of the *Central Patagonia Batholith*, individual plutons cannot be distinguished from adjacent igneous rock by mappable structures. Accordingly, the shape,

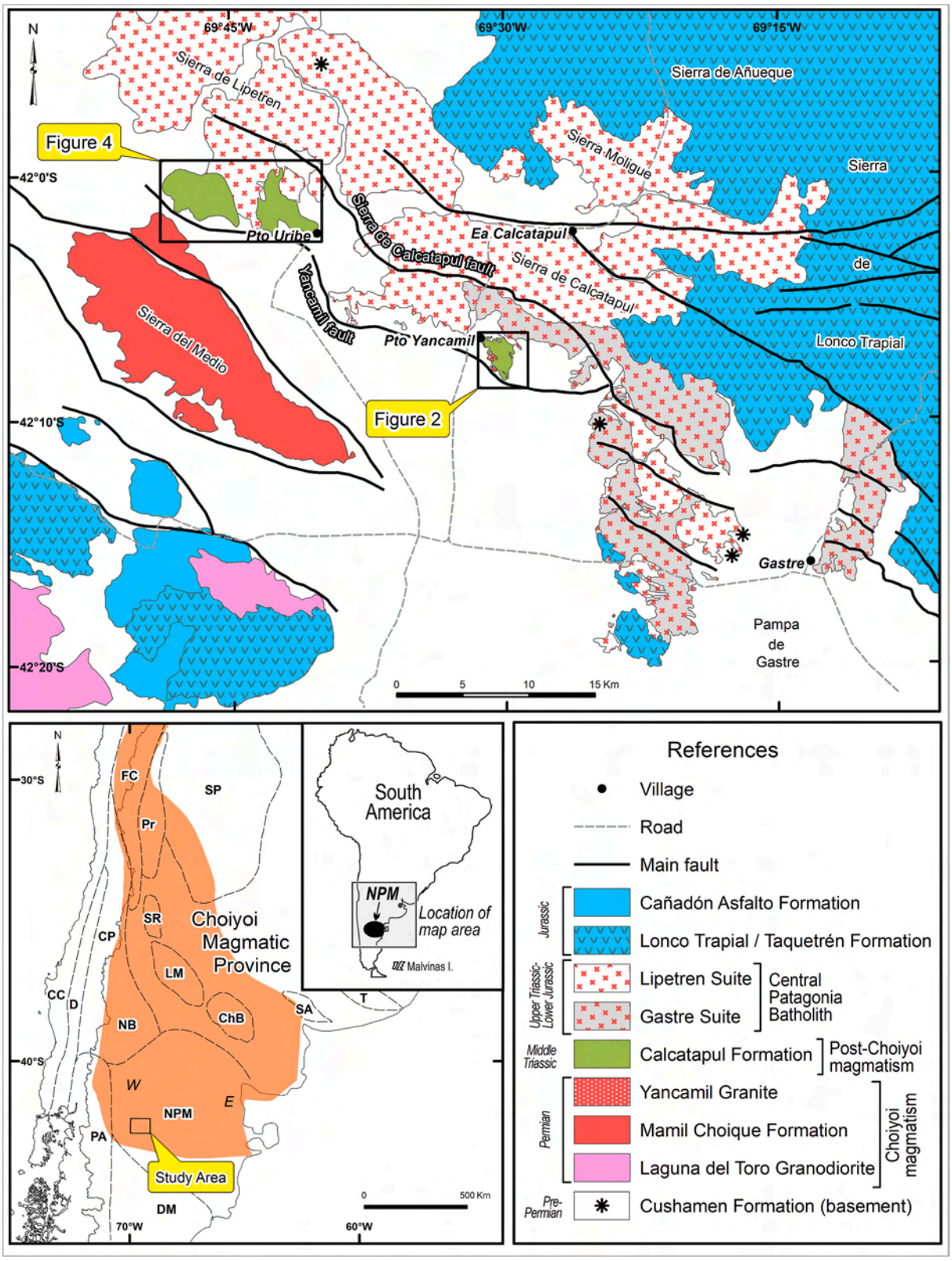

Fig. 1. Regional geological map of the southern parts of the North Patagonian Massif, depicting de Puesto Yancamil and Puesto Uribe areas along the south margin of the Sierra de Calcatapul. The inset shows the situation of the study area concerning the regional distribution of the Permo-Triassic Choiyoi Magmatic Province of the western Gondwana margin (modified from Sato et al., 2015). Morphostructural regions of Chile and Argentina: FC: Frontal Cordillera, Pr: Argentine Precordillera, SP: Sierras Pampeanas, CC: Coastal Cordillera, D: Central Depression, CP: Cordillera Principal, SR: San Rafael Block, LM: Las Matras Block, ChB: Chadileuvú Block, SA: Sierras Australes, T: Tandilia (Río de la Plata craton), NB: Neuquén Basin, PA: Patagonian Andes, NPM: North Patagonian Massif with (W) western and (E) eastern regions, DM: Deseado Massif.

areal extent, and dominant axis of the batholith assembled by the alignment of a group of plutons remain unclear, though the batholith emplacement has been interpreted as occurred along the NW-SE trending, transcontinental dextral transcurrent *Gastre Fault System* (Rapela et al., 1991, 1992).

The magmatic crystallization of the Lipetrén Suite is 215 ± 1 Ma (ICP-MS U–Pb zircon, Lagorio et al., 2015), thought minimum cooling or resetting ages of 208 ± 1 Ma (Rb–Sr whole rock, Rapela et al., 1992) and 206 ± 4 Ma (Ar–Ar biotite, Zaffarana et al., 2014) have also been reported. The magmatic crystallization of the Horqueta Granodiorite is 213 ± 2 Ma (ICP-MS U–Pb zircon, Lagorio et al., 2015), which is indistinguishable, within the error, from Ar–Ar biotite data of 213 ± 5 and 214 ± 2 Ma (Zaffarana et al., 2014) for the same Gastre Suite. Previous isotopic dating from this suite yielding 220 ± 3 Ma (Rb–Sr whole rock, Rapela et al., 1992) and 221 ± 1 Ma (U–Pb zircon, Rapela et al., 2005), suggests that at least parts of this group of intrusions are older, being regarded as the country rocks of the Lipetrén Suite (Rapela et al., 1992; Zaffarana et al., 2014). According to magmatic crystallization ages, the emplacement of Gastre and Lipetrén suites can be considered roughly synchronous within the Late Triassic.

The Calcatapul Formation and Lipetrén Suite are overlaying unconformably by a thick pile of volcanic rocks consisting of intercalations of andesitic-to-dacitic lava/pyroclastic flows, volcanic agglomerates, ashfall tuffs, and siliciclastic rocks with main pyroclastic inputs. The succession was gathered into either the Taquetrén Formation (Nullo and Proserpio, 1975; Nullo, 1978; Proserpio, 1978) or the Lonco Trapial Formation (Figari et al., 2015; Zaffarana et al., 2018; Lizuain et al., 2019, among others), their Ar–Ar minerals effusion age range is mostly between 192 and 178 Ma (Zaffarana and Somoza, 2012; Zaffarana et al., 2018). However, in light of a SHRIMP U–Pb zircon date of 242.9 ± 2.5 Ma obtained for the Taquetrén Formation at Sierra de Añueque area (Fig. 1; Franzese et al., 2002), the timing of the whole pile should be reconsidered. As these authors pointed out, the volcanic rocks assigned to the Taquetrén Formation includes, at least, Triassic and Jurassic magmatic events. Therefore, given the U–Pb date and based on the geological situation, a redefinition of the lithostratigraphic names, ages, and areal extent is needed, based on new mappings that support the original stratigraphic features between both volcanic successions.

4. Materials and methods

ASTER and Landsat satellite images, downloaded free from the United States Geological Survey *"Earthexplorer"* at https://earthexplorer.usgs.gov/, together with aerial photographs (1:50.000 scale) were used to prepare the geological maps of the Calcatapul Formation. Remote sensing techniques applied are described in Cábana and

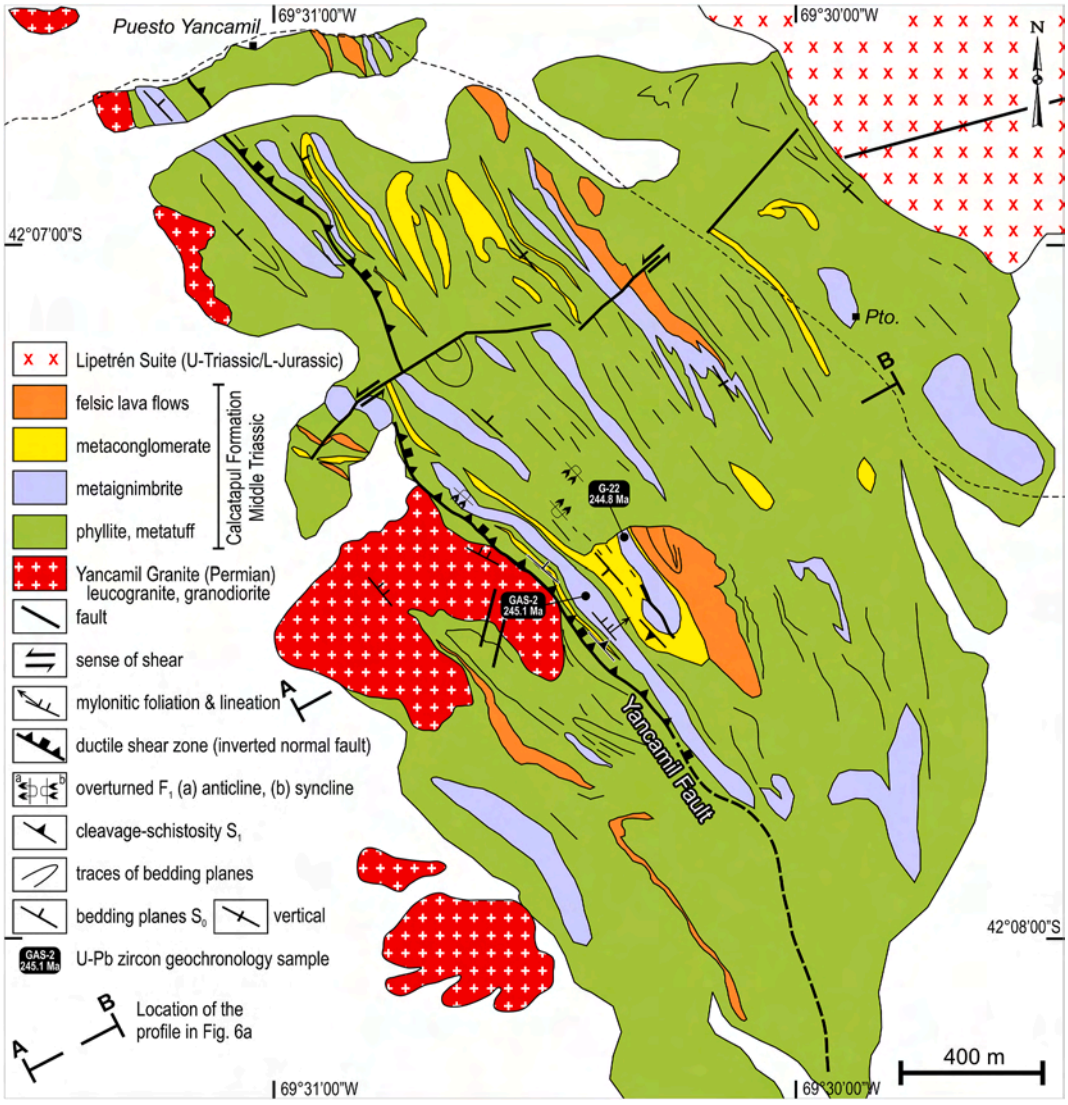

Fig. 2. Geological map of the Calcatapul Formation and the associated intrusions in the Puesto Yancamil area. For the figure location, see Fig. 1.

Marchionni (2011), Cábana et al. (2017), and references therein. Later, the maps were verified with field works.

The meta-ignimbrites GAS-2 and G-22 were selected for zircons study by LA-MC-ICPMS U–Pb method due to good outcrops and fresh samples. GPS and sample field locations are depicted in Table 1 of the Electronic Supplementary Materials and Fig. 2, respectively.

Zircon crystals were separated, starting from approximately 2.5 kg of each sample. For GAS-2, after jaw-crushing and sieving, zircons were concentrated by standard gravimetric and magnetic techniques in the Centro de Investigaciones Geológicas (UNLP-CONICET). Two zircon fractions (70 and 100 grains) were randomly hand-picked in alcohol under a binocular microscope (Fig. 3a–b). Mounting zircons into epoxy resin plugs, CL imaging, and U–Pb age determinations were carried out in the Geochronological Research Center (CPGeo, Geosciences Institute, University of São Paulo, Brazil). Thermo-Fisher Neptune laser-ablation multi-collector inductively coupled plasma mass spectrometer equipped with a 193 Photon laser system was used, with the operating conditions, instrument settings, and laser ablation system described in Sato et al. (2009, 2010). Zircon fractions mounted in different plugs were analyzed separately in two analytical sessions. The data were processed (reduction, age calculation, and plotting) with an in-house Excel® spreadsheet, based on ISOPLOT V3 formulas (Ludwig, 2003).

The U–Pb zircon analysis of the sample G-22 was performed in Activation Laboratories (Canada). After crushing, sieving, and concentration, representative zircon grains were hand-picked, mounted in epoxy resin, polished, and CL imaging. Resonetics RESOlution M-50 series 193 nm excimer laser ablation system equipped with a Laurin Technic Pty S-155 ablation cell was used, following the analytical procedure and off-line data reduction used by this laboratory (https://actlabs.com/). We represented the analytical results in Tera- Wasserburg diagrams and weighted means of overlapping and coherent $^{206}Pb/^{238}U$ ages using Isoplot/Ex (Ludwig, 2003). Full U–Pb zircon analytical results of samples GAS-2 and G-22 are presented in Table 1 of the Electronic Supplementary Materials.

5. Geology of the Calcatapul Formation

Two small outcrops of meta-volcanic rocks are located along the southern margin of the Sierra de Calcatapul at Puesto Yancamil and Puesto Uribe areas (Fig. 1). Until now, the Calcatapul Formation has not been recognized anywhere else in Patagonia (Volkheimer, 1965; Proserpio, 1978; Nullo, 1978; von Gosen and Loske, 2014).

5.1. Primary stratigraphic features and volcano-sedimentary protoliths

South of the Puesto Yancamil area, the Calcatapul Formation overlays the Yancamil Granite along its eastern margin. However, an intrusive contact of the pluton into the Calcatapul Formation was also argued (von Gosen and Loske, 2014). In turn, a pluton of the Lipetrén Suite intruded the already deformed-metamorphosed rocks of the Calcatapul Formation, at the foothill of the Sierra de Calcatapul, with sharp discordant contacts (Fig. 2).

The Calcatapul Formation consists of alternating beds of (meta-) ignimbrites, volcanogenic conglomerates, andesitic-to-dacitic lava flows, and tuffs, which defines the compositional banding S_0. It follows roughly parallel to the folded contact of the Yancamil Granite (Fig. 4a). The lack of contact metamorphic effects, e.g., hornfels, already detected by Proserpio (1978, p. 25), the absence of chilled margins along with the granite contact, in addition to granitic pebbles derived from the underlying rocks in ignimbrites and conglomerates (Fig. 4b), indicate that

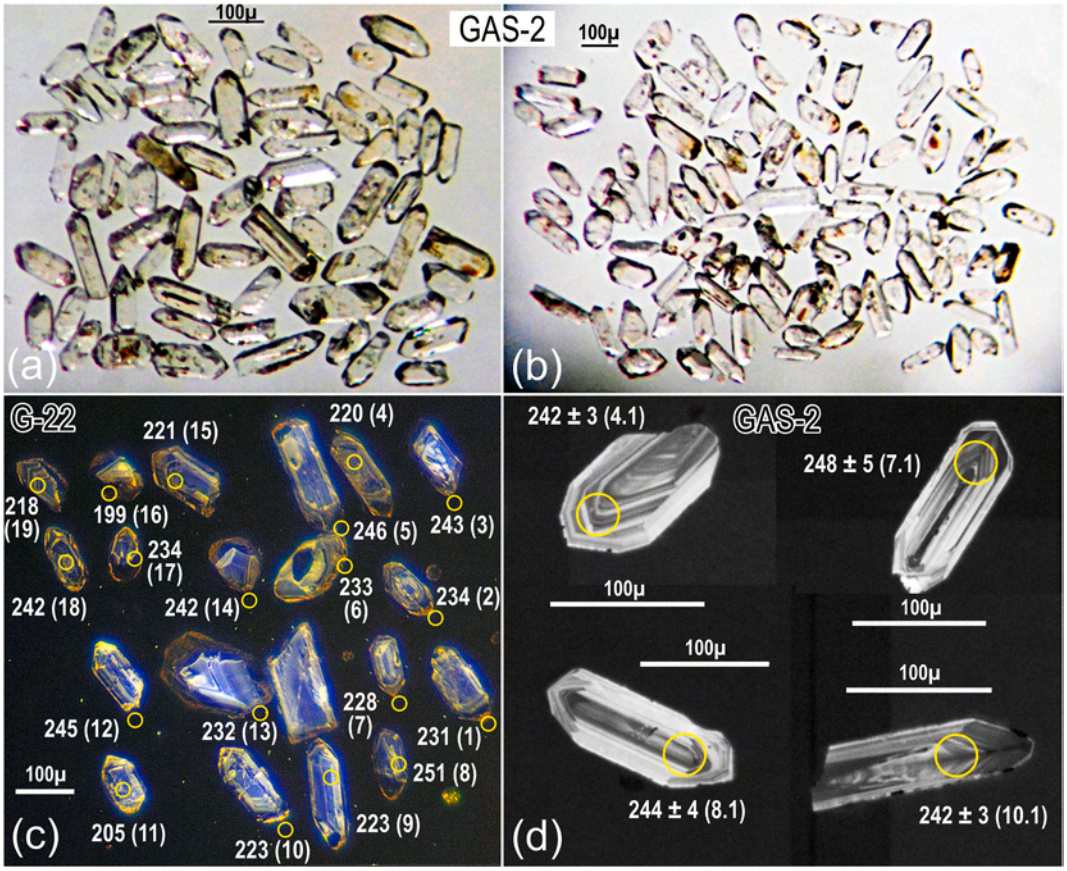

Fig. 3. **(a, b)** Photomicrographs under the binocular microscope of the two zircon fractions separated from meta-ignimbrite GAS-2. See details in the text. **(c, d)** Cathodoluminescence images of the full set of magmatic zircons from sample G-22 (c) and typical magmatic zircon crystals from GAS-2 (d), also indicating the analyzed spots with the $^{238}U/^{206}Pb$ ages obtained. The number in parentheses corresponds to the analytical spot depicted in Table 1 of the ESM.

Fig. 4. Field view of primary igneous features and D_1 structures in the Yancamil Granite and Calcatapul Formation from Yancamil (a–e) and Uribe (f–g) areas. **(a)** Non-conformity contact between both units. **(b–c)** Meta-ignimbrite GAS-2 contains a granitic clast of the underlying Yancamil Granite. S_1 schistosity mimics the igneous eutaxitic texture. **(d)** Thin strip with relic foliation folds in meta-ignimbrite GAS-2, wrapped by S_1 foliation planes. **(e)** Granitic boulder of the underlying Yancamil Granite in a meta-conglomerate bed. **(f)** Alternating beds of meta-ignimbrite (left) and meta-rhyolite (right) exhibit the S0/S1 structural relationship and the stretching lineation L_1 on S_1 planes. **(g)** Rhyolitic boulder of the consanguineous volcanism in a volcanogenic meta-conglomerate bed.

a primary non-conformity contact exists between volcanic protoliths of the Calcatapul Formation and Yancamil Granite.

Close to the contact, a nearly tabular ignimbrite bed readily distinguishable by uniform composition and traceable over outcrop distances resulted in a marker horizon for mapping and reconstructing the folded structure. The grayish-green ignimbrite displays a distinctive eutaxitic texture indicated by the welding of pumice clasts or *fiammes,* defining a discontinuous layering parallel to flow banding/foliation. Angular lithic volcanic- and crystal fragments of quartz and feldspars wrapped by flow foliation lines and flow folds are embedded in a recrystallized matrix (Fig. 4c, d, e). A lens-shaped bed up to 25 m thick of polymictic matrix-supported conglomerate is intercalated parallel to the ignimbrite bed. The volcanogenic conglomerate preserves a crude S_0 stratification. Its magmatic provenance of detrital components is revealed by sub-rounded to rounded pebbles to granules of andesites, dacites, devitrified pumices, pelites, and granitoids, with minor mono- and

polycrystalline quartz. The matrix is recrystallized to a phyllite with penetrative schistosity defined by chlorite-biotite alignment. The petrography of volcanic and granitic clasts is the same as those of the intercalating lava flows and underlying Yancamil Granite, respectively, therefore indicating a proximal setting connection with the volcano-pyroclastic source area.

A massive, thick coherent porphyritic andesitic-to-dacitic lava flow lies in contact with the conglomerate. It consists mainly of euhedral feldspars phenocrysts and minor quartz embedded in an aphanitic groundmass with flow-banded foliation.

Towards the northeast, a number of tabular beds of ignimbrites, conglomerate lense/s (?), and <1 m thick layers of pumice sandstone are

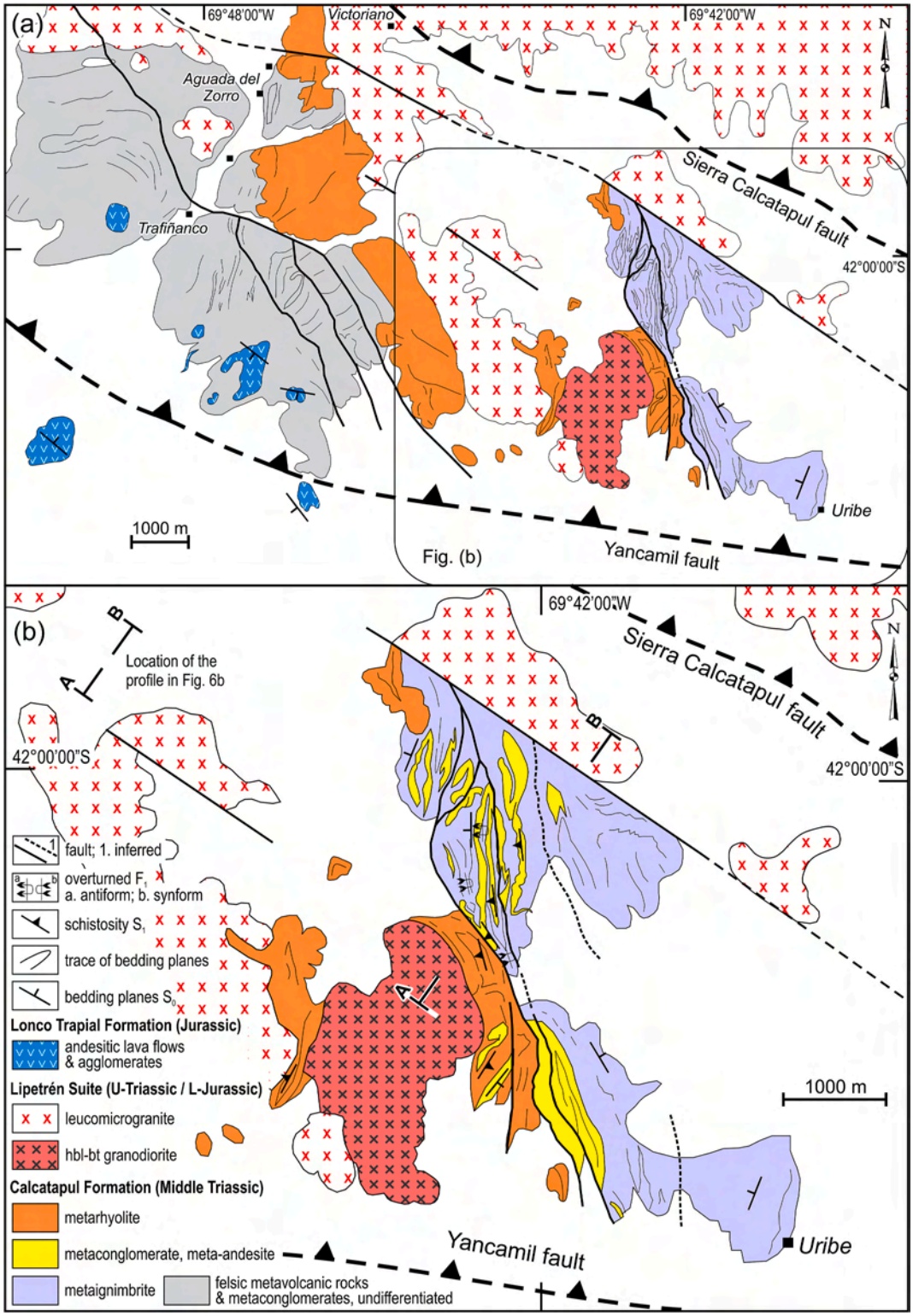

Fig. 5. Geological map of the Calcatapul Formation and the associated intrusions between the Aguada del Zorro and Puesto Uribe area. For the figure location, see Fig. 1. **(a)** The areal extent with outcrops of the unit in the northwestern part of the Sierra de Calcatapul is more extensive than previously estimated. **(b)** Geological and structural map of the Calcatapul Formation in the Puesto Uribe and surroundings. For the location, see Fig. (a).

intercalated in dark-grey phyllites. Juvenile tephra, quartz-feldspar crystal fragments, and volcanic lithics predominating over sedimentary clastic components indicate that phyllites could have formed from finely grained tuffs or clayey tuffite rather than shales or mudstones.

In the Puesto Uribe area, the Calcatapul Formation is intruded by a hornblende-biotite granodioritic pluton and several leucogranite bodies belonging to the Lipetrén Suite. Further west, the Calcatapul Formation is overlaid by andesitic lava-flows and agglomerates of the Lonco Trapial Formation unconformably (Fig. 5). Although the volcano-sedimentary sequence is the same as that of the Puesto Yancamil area, the alternating ignimbrite-conglomerate beds and lava flows are thicker, whereas phyllite-pumice sandstone succession, thinner. Besides, the matrix-supported conglomerates are coarser grain and composed of angular to sub-rounded cobbles and pebbles of volcanic rocks and granitoids (Fig. 4f–g). Yet, the lava-flows include more silica-evolved volcanic products, and either tabular or dome-shaped bodies of foliated rhyolites resemble that of shallow level intrusions, e.g., dikes and cryptodomes, that cut their comagmatic pyroclastic deposits.

5.2. D_1 structures

Within the Calcatapul Formation south of the Puesto Yancamil, the overprinting structural relationship between S_0–S_1 planes in the marker horizons allows reconstruction of the limbs and hinge zones of the folded rocks. Although no way-up structural indicators were found, it is reasonable to assume younging upwards of the relative ages of beds within the folded sequence, considering its simply deformed pattern.

The volcano-sedimentary compositional banding S_0 is folded as overturned tight F_1 anticlines and synclines of the decameter scale of SW-directed vergence. S_0 is NW-SE trending and dips steeply (>80°) to the NE, whereas axial plane cleavage S_1 is parallel to S_0 and dips less steeply (70–80°) also to the NE. NW-SE striking fold axes B_1 plunge gently to the SE (Fig. 6a). On S_1 planes, L_1 stretching lineation plunges either ~55° to WNW or ~85° to NE and is defined by the alignment of sericite-biotite aggregates and pressure shadows at crystal fragments and clasts. D_1 deformation also flattened and stretched pumice clasts parallel to L_1 lineation, resulting in an S-L fabric that mimics primary eutaxitic texture. According to the northeastward-dipping S_0–S_1 planes and the SW-directed verging overturned folds F_1, the folded belt displays

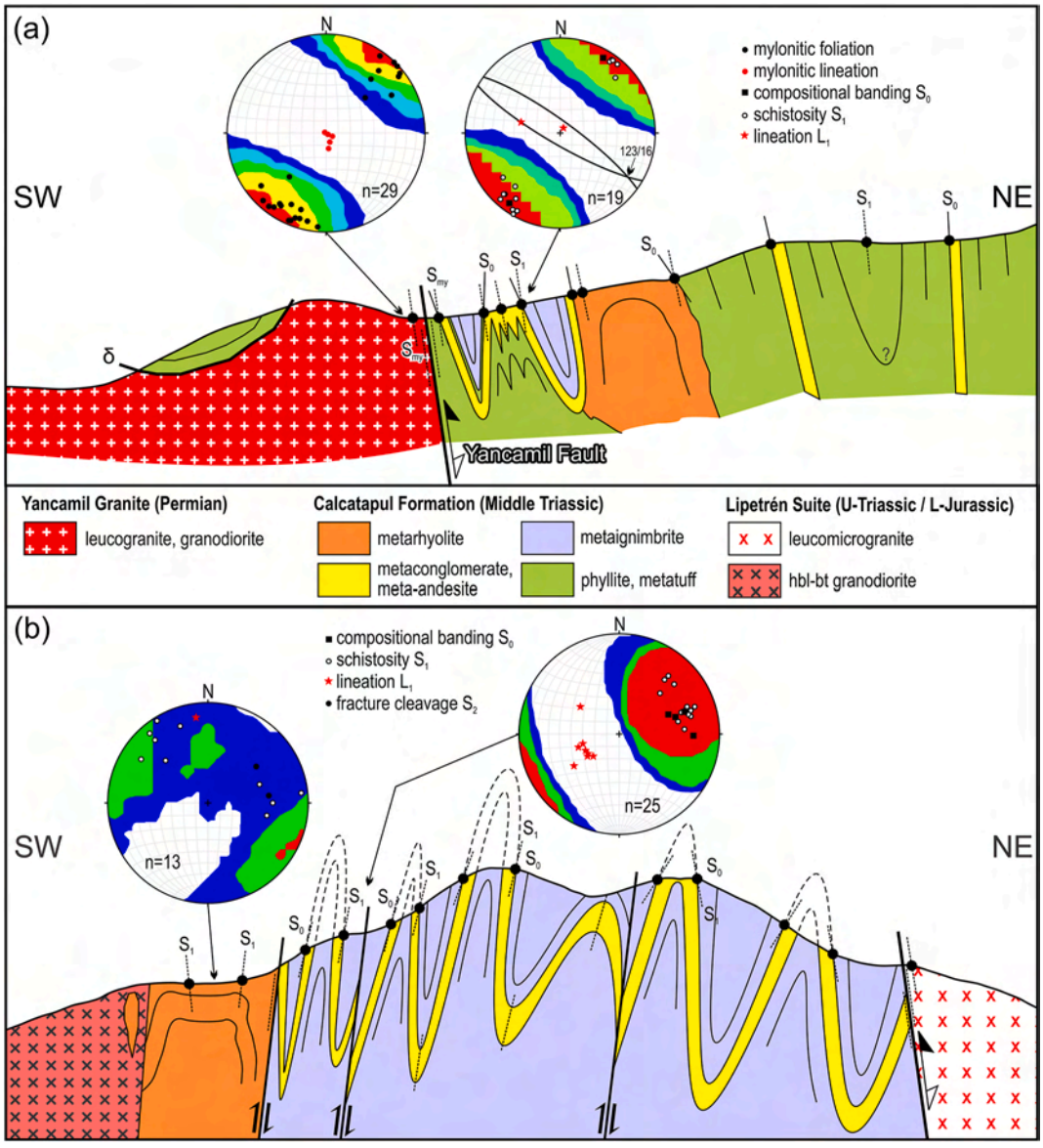

Fig. 6. (a, b). NE-SW trending geological cross-section exhibiting the D_1-D_2 structures of the Calcatapul Formation in the puestos Yancamil and Uribe, respectively. See the profile locations in Figs. 2 and 5b. Stereoplots are lower hemisphere, equal-area projections of poles. Contour intervals at 2% per 1% area.

a southwestward tectonic transport.

During D_1 contraction in the Yancamil Granite, the heterogeneous deformation resulted in highly sheared contact and margins, alternating with less deformed parts towards inner zones. The interaction between the hard, more competent granite and the incompetent volcano-sedimentary cover resulted in localized flexural shearing along with the primary non-conformity contact. Thin strips of granitic and ignimbritic mylonites developed parallel to both sides of the contact, describing an NW-SE trending and northeastward dipping brittle-ductile shear zone <5 m width. It consists of a heterogeneous S/C fabric comprising sigmoidal S_0–S_1 planes displaced by discrete NW-SE trending shear C_1 planes of mylonitic foliation, which dips between near vertical and high-angles to either the NE or SW (Figs. 6a and 7a). On C_1 planes, a mostly NE or SW steeply plunging to sub-vertical mylonitic stretching lineation developed. Sigma- and delta-shapes of crystal feldspars fragments and pumice clasts, S/C fabric, and asymmetric pressure shadow at feldspar porphyroclasts indicate a top-to-the SW sinistral sense of shear parallel to mylonitic lineation (see also the field observations of von Gosen and Loske, 2014). In less mylonitized outer parts of the shear zone, the mylonitic foliation records continuous transitions into the axial plane cleavage S_1, with L_1 stretching lineation plunging in the same way as mylonitic lineation (Fig. 7b).

Within the Calcatapul Formation northwest of the Puesto Uribe, the S_0 volcano-sedimentary banding is folded and faulted around NE-directed vergence, overturned tight-to-isoclinal F_1 folds, and faults. The NW-SE trending S_0 planes are parallel to axial plane cleavage S_1 and dip steeply to the SW (Fig. 6b). On S_1 planes, L_1 stretching lineation plunges 55–62° mostly to SW.

Several NNW-trending faults are diagonal to the main NW-SE trending and northeastward dipping Sierra Calcatapul and Yancamil faults that bounded the outcrops of the Calcatapul Formation to the north and south, respectively (Fig. 5a, see also Giacosa et al., 2020). They are curved and anastomosing high-angle reverse faults that lie parallel to S_0–S_1 planes and also dip to the SW. According to the southwestward-dipping S_0–S_1 and fault planes and the NE-directed verging overturned folds F_1, the fold-and-fault belt displays a northeastward tectonic transport, with an opposite vergence to that of the Puesto Yancamil.

5.3. D_2 structures

The D_1 structures on the Yancamil Granite and Calcatapul Formation of the Puesto Yancamil are displaced by an orthogonal, steeply inclined to the sub-vertical left-lateral brittle strike-slip fault of the D_2 tectonic event, which also cut the Lipetrén Suite (Fig. 2). It is associated with a conjugate set of NW-SE (N 305/37° NE) and NE-SW (N 28/71° NW) trending, sinistral and dextral, closely spaced fracture cleavage S_2 (Fig. 7c), which is also distinctive in the meta-ignimbrites from west of the Puesto Uribe (Fig. 6b). On both surfaces, stepped slickensides with slickenfibres depict the relative sense of shear. These are the first deformational structures in the Lipetrén Suite, which intruded the D_1 structures of the Calcatapul Formation. The conjugate set is also associated with C_2 shear planes (Fig. 7d) following the same geometry and kinematics, which is also supported by the field observations of von Gosen and Loske (2014).

5.4. Micro-fabrics and metamorphism

In the meta-ignimbrites, relic pyroclastic features are eutaxitic texture, pumices, and andesitic/dacitic lithoclasts, six-sided euhedral quartz, and crystal fragments of plagioclase, sanidine, and biotite (Fig. 8a). Apatite and zircon are accessories. The composition is variable between dacite and rhyolite. The quartz is embayed, contains inclusions of biotite and devitrified matrix, and undulose extinction. Key metamorphic assemblages M_1 are chlorite-muscovite-opaque minerals replacing igneous biotite pseudomorphically and patches of sericite-zoisite-pistacite-albite overprinting feldspars. Lens-shaped fiammes mark the S_1 cleavage planes and are now recrystallized into irregular to

Fig. 7. Field view of the D_1 and D_2 structures in the Yancamil Granite (a–b) and Lipetrén Suite (c–d), respectively, from the Puesto Yancamil area. **(a)** S–C fabric in granitic mylonites from outer parts of the granite, near the contact with the country-rock of the Calcatapul Formation. **(b)** S_1 foliation in less deformed inner parts of the granite. **(c)** The conjugate set of spaced fracture cleavage S_2. **(d)** Outcrop-scale sinistral shear band associated laterally with S_2 planes.

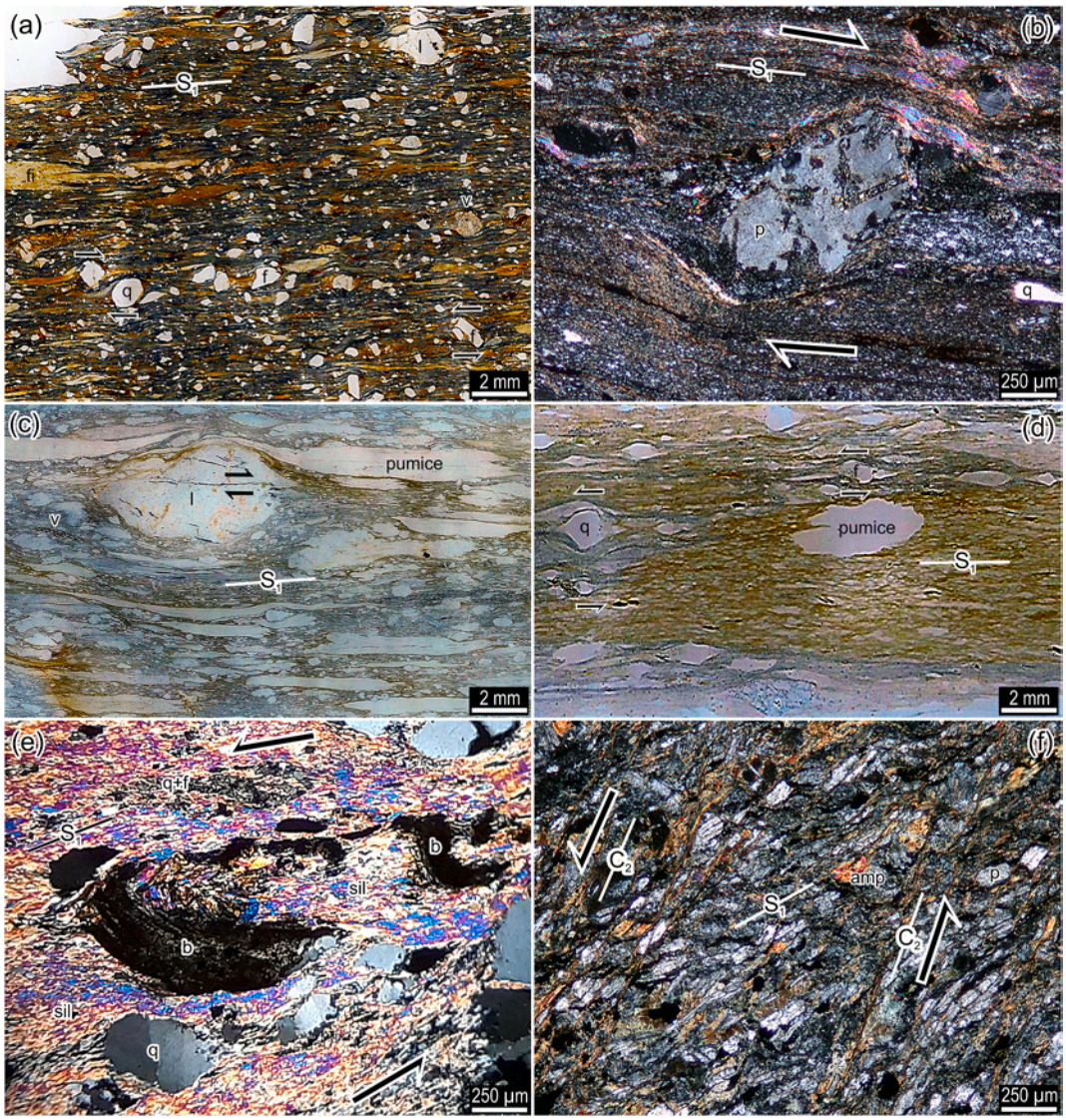

Fig. 8. Photomicrographs from thin sections, parallel and crossed polarizers, of the Calcatapul Formation (a-d, and f) and the Yancamil Granite (e). Figures (a), (c), and (d) are views of scanned thin-sections. **(a)** S_1 schistosity is parallel to the eutaxitic texture marked by flattened pumices or fiammes (fi). "f" and "q" is crystal fragments of feldspars and quartz, respectively, whereas "v" mark a volcanic lithic clast composed of porphyritic andesite. Both the dextral and sinistral sense of shear is also indicated in pressure shadows on them. **(b)** Magmatically corroded crystal fragment of plagioclase (p) wrapped by S_1 foliation planes and with pressure shadows exhibiting a dextral sense of shear in a meta-rhyolite. S_1 planes marked by recrystallized aggregates of quartz + feldspars. q: quartz fragment. **(c)** Matrix of a meta-conglomerate exhibiting flattened pumice and lithic (l) clasts surrounded by S_1 schistosity. See also the flattened volcanic clasts (v) with relict andesitic texture. **(d)** Phyllite exhibiting a recrystallized matrix composed predominating of micro-biotite (brown bands) and minor chlorite (green bands), also accompanied by flattened pumices parallel to S_1 schistosity and porphyroclasts of quartz (q) and feldspars (f), both with pressure shadows indicating a sinistral sense of shear. **(e)** High-grade granitic mylonite exhibiting quartz porphyroclasts (q) and a matrix composed of prisms and needles of sillimanite (sil) defining the mylonitic foliation (S_1), together with recrystallized quartz and k-feldspar aggregates (q + f). Micro-folded biotite and biotite fish (b), with dusty opaque intracrystalline aggregates, indicate a sinistral sense of shear. **(f)** S–C fabric in a mylonitized andesite from the Puesto Uribe area. Sigmoidal foliation S_1, displaced by discrete shear C_2 planes (=mylonitic foliation), and tremolite-actinolite prisms are defining both the D_1 and D_2 structures, also indicating greenschist facies conditions. Sinistral sense of shear. Minerals: p: plagioclase, amp: tremolite-actinolite.

a polygonal granoblastic aggregate of quartz-albite-biotite-chlorite-epidote. The matrix is also recrystallized to a fine-grained metamorphic inter-schistose assemblage M_1 composed of quartz-albite-sericite aggregate, aligned parallel to flattened fiammes. The S_0 bedding exhibit mylonitic fabric only along contacts, whereas most parts display heterogeneous solid-state deformation (see additional petrographic descriptions in Pezzutti and Busteros, 1975 and von Gosen and Loske, 2014).

Porphyritic dacite-to-rhyolite lava flows display variably sized phenocrysts of plagioclase, sanidine (?), and quartz affected by stretching and dynamic recrystallization. They are embedded in a matrix of recrystallized quartz-albite-K-feldspar-sericite/muscovite-chlorite-biotite ± epidote M_1 metamorphic assemblage, which alignment defines the S_1 cleavage planes (Fig. 8b). The intra-crystalline deformation of phenocrysts is distinguished by deformation lamellae, undulose extinction, and sub-grains in quartz, and kinked or tapered albite twins towards the grain boundary in plagioclase. Pressure shadows are filled with quartz, sericite, and chlorite, indicating both dextral and sinistral shear sense.

Within the granolepidoblastic matrix of metaconglomerates, the magmatic provenance of detrital components is revealed by clasts of andesites, dacites, and rhyolites, recrystallized pumices, and minor granitoids (Fig. 8c). Clasts' compositions are the same as those lava flows intercalated in the same sequence. Crystal fragments of plagioclase

and quartz exhibit undulose extinction and sub-grains. Six-sided crystals also indicate the volcanogenic origin of quartz grains with embayment and rounded inclusions of the groundmass. The schistose matrix consists of recrystallized quartz-chlorite-sericite/muscovite ± biotite M_1 assemblage, which defines the S_1 cleavage planes together with lens-shaped and flattened pumice clasts. The matrix also contains heavy minerals, e.g., zircon, apatite, rutile, and opaque.

Phyllites were also derived from volcanogenic rocks and consisted mainly of fragments of angular quartz and feldspars and very fine-grained pumice clasts embedded in a matrix recrystallized into quartz-sericite/muscovite-chlorite-micro-biotite M_1 assemblage (Fig. 8d). Pumices are flattened, stretched, and recrystallized to sericite/muscovite, and together with the alignment of mica aggregates, define the schistosity S_1. Pressure shadows are filled with quartz-sericite-chlorite ± biotite assemblage.

The Yancamil granite exhibits heterogeneous solid-state deformation, high-grade metamorphic conditions, and mylonitic fabric, which are temporal-spatially related to those of the volcano-sedimentary pile of the Calcatapul Formation. Fine-to-medium grained mylonites exhibit porphyroclasts of K-feldspar, quartz, and biotite embedded in an inter-schistose matrix. Feldspar porphyroclasts show undulose extinction, kinked perthites, and core-mantle structures due to partial recrystallization, mostly in pressure shadows. Both dextral and sinistral sense of shear is indicated by biotite fishes, stair-stepping across the porphyroclasts, and S/C fabric. It is worth noting the double sense of shear, not only in mylonites but also in meta-volcanic rocks. Quartz porphyroclasts with undulose extinction also shows sub-grain development. The matrix consists of alternating parallel bands of small, fully recrystallized quartz, K-feldspar, micro-biotite, and short-prism of sillimanite showing granoblastic texture, and bands of muscovite, sillimanite fibers, and biotite with schistose texture, both defining the mylonitic foliation (Fig. 8e).

The penetrative S_1 foliation planes in the S/C fabric of the mylonitized meta-volcanic rocks are heterogeneously affected by the C_2 shear planes (Fig. 8f). Both the S_1 and the C_2 planes are composed of the same metamorphic mineral assemblage M_1, and then they grew under the same metamorphic conditions.

6. Geochronology

6.1. Previous geochronological study

Previous radiometric studies reported an ID-TIMS U–Pb zircon date from Yancamil Granite (von Gosen and Loske, 2014). Five concordant $^{206}Pb/^{238}U$ ages scatter between 262.8 and 279.9 Ma, and the calculated Discordia of this cluster yielded a lower intercept at 272 ± 10 Ma (MSWD 15). Another age of 335.5 Ma, though discordant, was considered as a zircon inheritance from the country-rock (Cushamen Formation?). When forced through a lower intercept of 0, the same cluster yielded an upper intercept at 261 + 16/-17 Ma (MSWD 0.33), which was interpreted as the likely minimum age of the Yancamil Granite (von Gosen and Loske, 2014).

6.2. Results of the LA-ICPMS method

Meta-ignimbrite GAS-2: The collected zircon fractions are euhedral, bi-pyramidal short-to-long prisms with well-defined faces, partly either remarkably well-preserved vertices/edges or with little roundness and aspect ratio 1.5:1 to 2–4:1. Their lengths range between 100 and 150 μm, but few fragments of the large prisms are shorter. Zircons are generally clear, almost colorless, but some inclusions are present, partly elongated parallel to the c-axis, whereas others are globule and irregular (Fig. 3a–b).

The CL images of 31 analyzed zircon grains show well-developed oscillatory growth zoning and parallel sector zoning that, along with morphology and high Th/U values are typical magmatic features (Fig. 3d, Hoskin and Schaltegger, 2003). Considering the two zircon fractions together, fifteen out of thirty-one points define a Concordia age of 245.1 ± 2.8 Ma, with MSWD 0.26. The same cluster of the fifteen concordant zircons (Th/U ratio 0.15–1.97) yielded a weighted $^{206}Pb/^{238}U$ mean age of 244.7 ± 3.8 Ma (MSWD 3.8, Fig. 9a–b). There are four inheritance ages of 292 ± 4, 276 ± 3, 274 ± 3, and 264 ± 4 Ma (magmatic grains with Th/U 0.13–1.25). At the same time, four zircons have younger $^{206}Pb/^{238}U$ ages scattering between 233 and 214 Ma, although with significant errors, high common Pb, and high discordances ≫10%. The remaining zircon spots were discarded due to high common Pb, significant errors, and/or spurious analytical results (Table 1 of the ESM).

The four inherited spots are concordant and yielded a weighted $^{206}Pb/^{238}U$ mean age of 275.5 ± 8.5 Ma (MSWD 1.08). Within error, this Permian age is indistinguishable from the weighted $^{206}Pb/^{238}U$ mean age of 272 ± 14 Ma (MSWD 0.23) to Yancamil Granite (Fig. 10), recalculated with the ID-TIMS U–Pb zircon analytical data from Table 1 of von Gosen and Loske (2014).

Meta-ignimbrite G-22: The CL images of 19 analyzed zircon grains show well-developed oscillatory growth zoning in bright luminescence inner zones and parallel sector zoning in dark luminescence outer zones/rims (Fig. 3c). The Th/U ratios ranging mostly between 1.02 and 2.12 are unusually high to magmatic zircons.

The data set overlaps within their assigned errors having more than one age-component. Then two clusters of concordant zircons can be deconvoluted (Fig. 9c) using the "unmix ages" function of Isoplot/Ex (Ludwig, 2003). A cluster of five points define a Concordia age of 244.8 ± 4.1 Ma, with MSWD 8.7, and a weighted $^{206}Pb/^{238}U$ mean age of 244.6 ± 4.7 Ma (MSWD 2.6). The second cluster of eight concordant points defines a weighted $^{206}Pb/^{238}U$ mean age of 226.7 ± 4.4 Ma (MSWD 8.3; Fig. 9d–f). The $^{206}Pb/^{238}U$ ages of the remaining zircon spots scattered between 242 and 199 Ma and were discarded due to high common Pb ≤ 8.2% and discordances ≤48.5% (Fig. 9d, Table 1 of the ESM).

7. Discussion with interpretations

7.1. Timing of magmatic crystallization, deformation, and metamorphism

Original stratigraphic features and U–Pb ages indicate that the Calcatapul Formation is younger than Early-Middle Paleozoic, as previously suggested. The U–Pb zircon Concordia ages of 245.1 ± 2.8 and 244.8 ± 4.1 Ma constrain their magmatic crystallization to Anisian, Middle Triassic (Fig. 9). Within their errors, the ages are indistinguishable from each other. Then, given the folded structure of the Calcatapul Formation, it is reasonable to assume that samples GAS-2 and G-22 dated could be part of the same ignimbrite bed (Figs. 2 and 6a).

For the meta-ignimbrite G-22, the additional mean $^{206}Pb/^{238}U$ date of 226.7 ± 4.4 Ma can be interpreted as the age of the subsequent deformation-metamorphism D_1-M_1 event by Norian, Upper Triassic. Although the analyzed spots in the magmatic zircons that contributed to this younger cluster come from cores and rims, and therefore an unambiguous age of metamorphic recrystallization at the rims cannot be highlighted, dark luminescence areas with very high Th/U ratio (1.02–2.12, Table 1 of the ESM) in these zircons can likely be ascribed as effects of crystal-plasticity growth under deformation-related processes (e.g., Timms et al., 2006; Möller and Kennedy, 2006). Nevertheless, a detailed microstructural study of zircons (EBSD) is needed to substantiate evidence of the relative enrichment of Th over U by enhanced bulk-diffusion of these elements during the D_1-M_1 event. Then, allowing for the magmatic crystallization ages, the 226.7 ± 4.4 Ma date point towards some post-crystallization modification or resetting on the bulk U–Th–Pb system of magmatic zircons as the result of the tectono-metamorphic overprint D_1-M_1.

U–Pb geochronological data of the underlying and overlying units agree with the new-fangled U–Pb ages informed here to Calcatapul

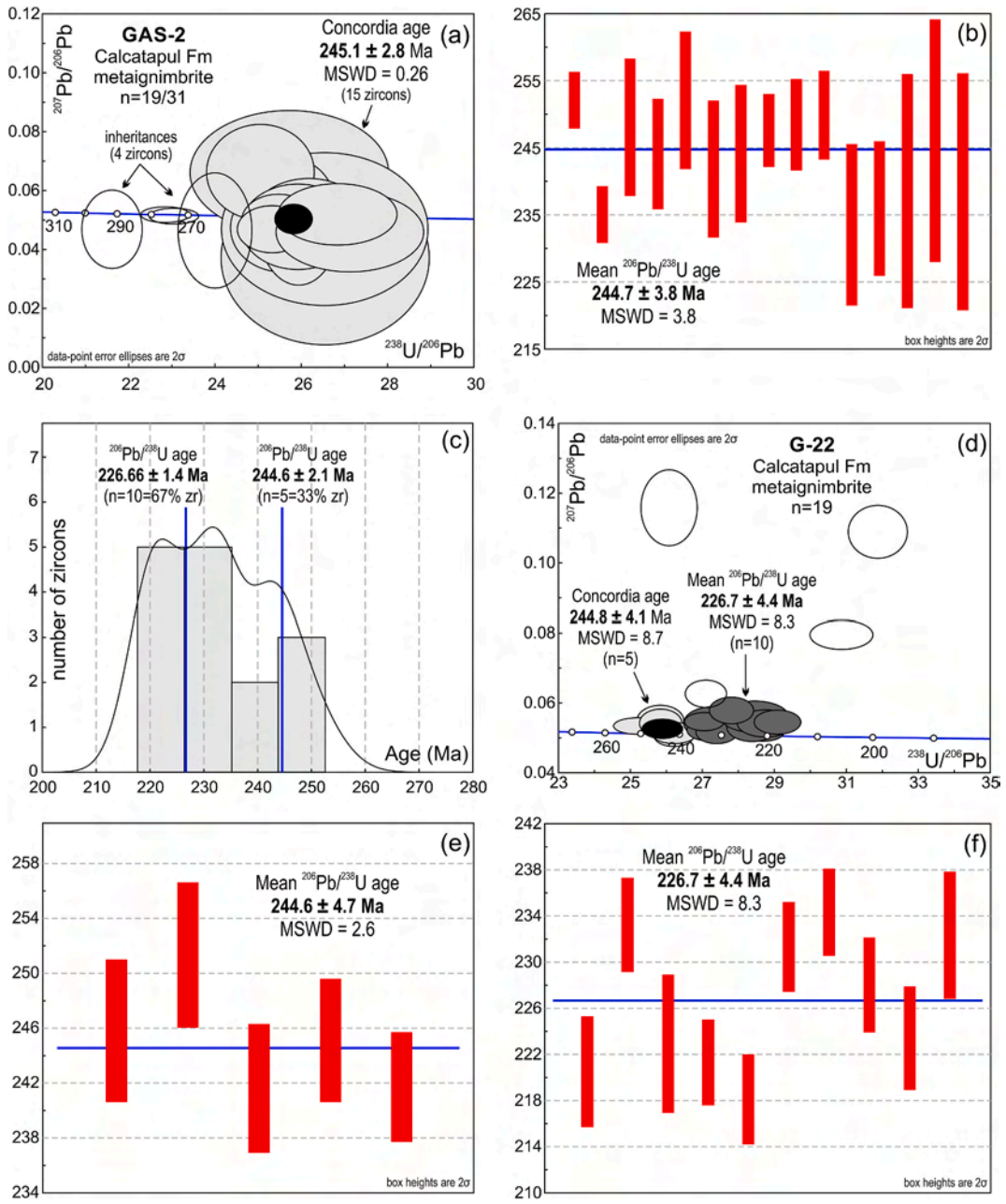

Fig. 9. Concordia diagrams of zircon data from meta-ignimbrites GAS-2 **(a)** and G-22 **(d)**. $^{206}Pb/^{238}U$ ages of those spots that were used to derive the weighted mean age of samples GAS-2 **(b)** and G-22 **(e–f)**. Error bars show the standard deviation for each spot age. **(c)** Unmix ages diagram performed with Isoplot/Ex (Ludwig, 2003) depicting the two zircon age-components of sample G-22.

Formation. In the meta-ignimbrite GAS-2, the zircon inheritance age of ~275 Ma is indistinguishable, within error, from the magmatic crystallization of the underlying Yancamil Granite that occurred at ~272 Ma (Fig. 9, see also Fig. 10a of von Gosen and Loske, 2014). Therefore, the Yancamil Granite was already exhumed at the time of the deposition of the Calcatapul Formation and was the most likely source area of the granitic clasts enclosed by the ignimbrite (and also conglomerates), and from where the inherited magmatic zircons would derive.

On the other hand, the top stratigraphic constraint is provided by the emplacement of igneous bodies belonging to Lipetrén Suite and Horqueta Granodiorite, which occurred between 215 and 213 Ma (Zaffarana et al., 2014; Lagorio et al., 2015), into already deformed and metamorphosed Calcatapul Formation. Younger Rb–Sr and Ar–Ar ages of 208–206 Ma on the same granitoids (Rapela et al., 1992; Zaffarana et al., 2014) point towards a Rhaetian isotopic resetting of the Lipetrén Suite and its country rocks owing to overprinting deformation D_2. K–Ar whole rock/biotite ages of 202–203 Ma (Stipanicic et al., 1968; Stipanicic and Linares, 1969; Lesta et al., 1980) can be ascribed as dating the same isotopic resetting due to D_2 event.

7.2. *Volcano-sedimentary depositional setting concerning tectonics*

Towards the base and top, the volcano-sedimentary pile of the Calcatapul Formation is limited by stratigraphic/structural discontinuities. It lay above and was deposited on the pre-existing eroded granitic rocks of the Yancamil Granite, representing the Gondwanide magmatic cycle in the Gastre area. This indicates a significant hiatus, which includes important uplift and erosion to expose the igneous-metamorphic rocks of the Gondwanide orogen, and then leveling the basement ridges and hills. This unconformity has regional distribution in the southwestern

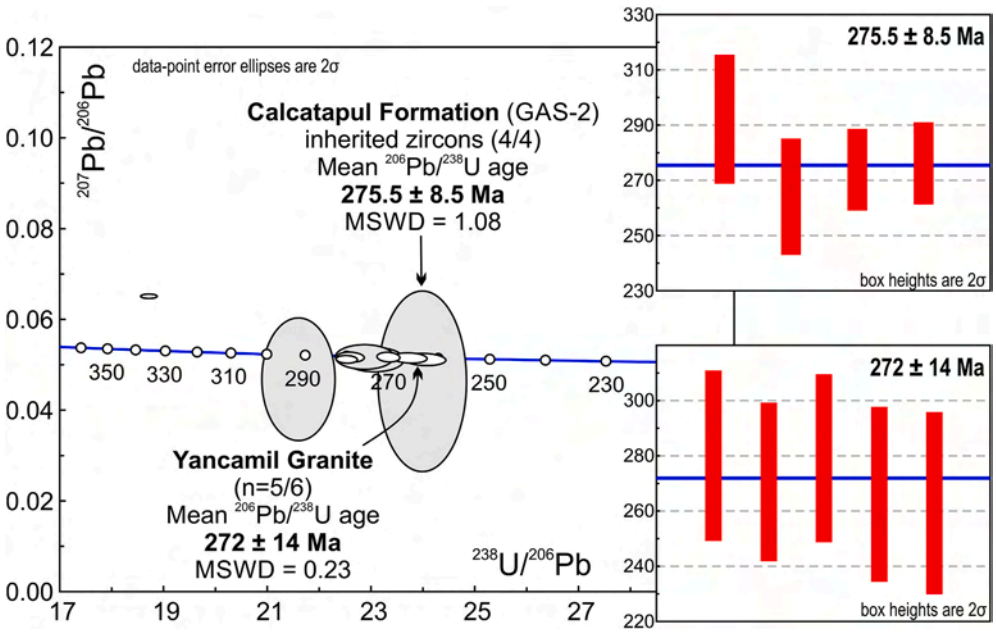

Fig. 10. Concordia diagram of inherited zircon data from meta-ignimbrite GAS-2 and zircon data from Yancamil Granite recalculated with the analytical data of Table 1 from von Gosen and Loske (2014). Insets show $^{206}Pb/^{238}U$ ages of those spots used to derive the weighted mean age, and error bars show the standard deviation for each spot age.

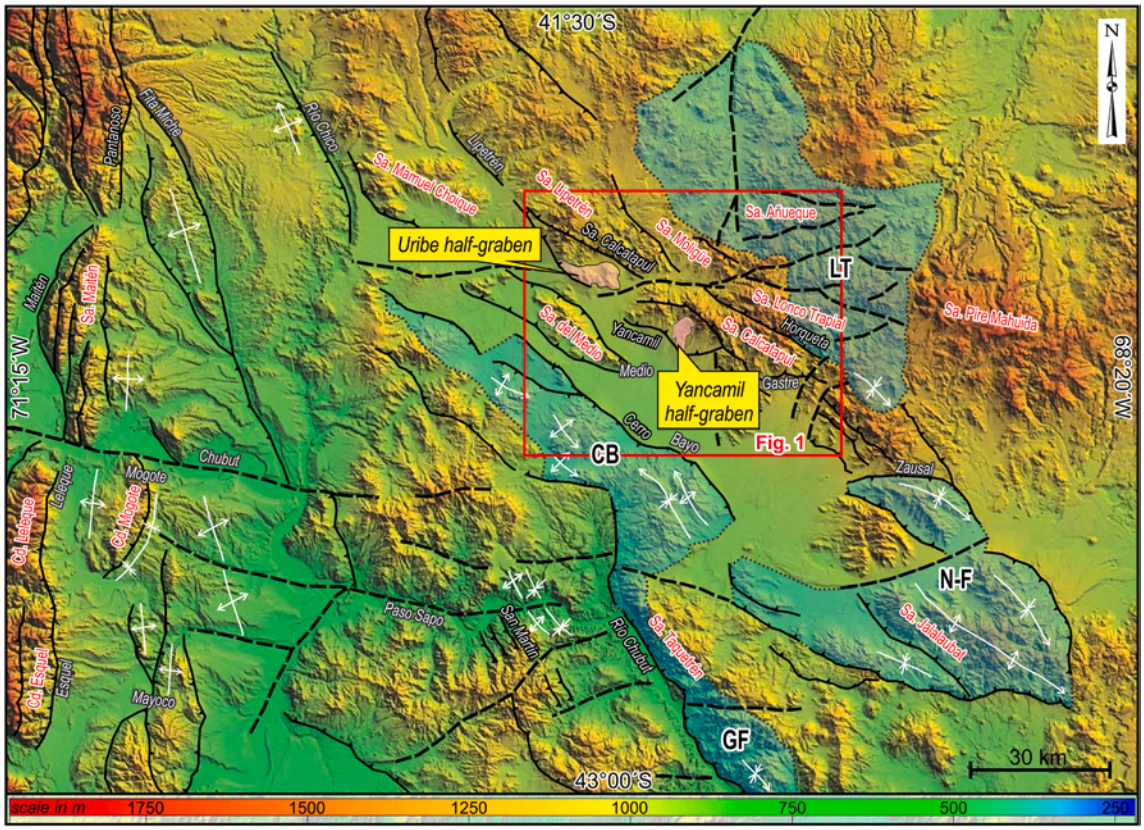

Fig. 11. Structural map of the Sierra de Calcatapul area and surroundings (modified from Giacosa et al., 2020), showing the main ranges bounded by master NW-SE trending reverse faults. The main folds are parallel to the reverse faults and located in the hanging-walls. The Uribe and Yancamil half-grabens are situated towards the northeast along the inverted Yancamil fault placed southward. The subsequent Jurassic rift depocenters are also associated with reverse faults. The Jurassic inverted rifts are CB: Cerro Bayo, LT: Lonco Trapial, GF: Gorro Frigio, and N–F: Navidad-Fossatti. Near E-W trending regional lineaments decouple the NW-striking structures. The base image is a digital elevation model downloaded from NASA's Shuttle Radar Topography Mission, SRTM Worldwide Elevation Data (90 m, three arc-second resolution). Web-site: https://www2.jpl.nasa.gov/srtm/.

margin of Gondwana, extending from the main Andean Cordillera (e.g., "Cordillera Frontal") southward, through Neuquén Basin-San Rafael Block into Patagonia. It is the so-called "*Huárpica unconformity*" formed by the "*Huárpica extensional phase*" of the Early Triassic age (see the synthesis of Leanza, 2009; Llambías and Sato, 2011). Even though each area is characterized by its specific stratigraphy, lithology, and structural levels, the Huárpica phase is recorded as representing the culmination of the extensional orogenic collapse that followed the San Rafael compressive phase of the Gondwanide Orogen (Azcuy and Caminos, 1987; Ramos, 1988). The minimum U–Pb age of ~261 Ma to Yancamil Granite, assuming recent Pb-loss (von Gosen and Loske, 2014), could represent the maximum age for the granite uplift and exhumation before the orogenic collapse.

Related to termination of the extensional collapse of Gondwanide orogen, the deposition of the volcano-sedimentary pile of the Calcatapul Formation could have taken place in small NNW-SSE trending basins, on a pre-rift basement represented by the Yancamil Granite. The isolated depocenters, which shall be named Yancamil and Uribe, have typical half-graben geometry (Fig. 11). As can be seen in the Puesto Yancamil outcrops (Fig. 2), the basin-bounding fault on the west side of the half-graben is a NE-dipping high-angle fault. The NNW-SSE orientation of the fault, in turn, is oblique to the NW-SE trending major Yancamil and Sierra de Calcatapul faults (Giacosa et al., 2020). The intercalation of pyroclastic rocks, lava flows, and sedimentary deposits containing main volcaniclastic inputs could represent the infill pattern of a syn-rift sequence. The clastics were also supplied by the granitic basement of the rift shoulders from the southwest.

Owing to the volcano-sedimentary pile are dominated by several facies of effusive and explosive rocks with minor alluvial volcanogenic conglomerates, also associated to sub-volcanic cryptodomes intruding their consanguineous deposits, indicates the occurrence of composite sub-aerial volcanoes at the boundaries of the half-grabens (McPhie et al., 1993; Gifkins et al., 2005).

Fault tectonics related to the formation of horst-and-graben structures seem to be likely further west of the Sierra de Calcatapul at the Sierra del Medio area (Figs. 1 and 11), as noted by Volkheimer (1965, 1973) and Llambías et al. (1984). The overall setting of normal fault tectonics and magmatism has been related to the Triassic initial phase of rifting, which produced NW-SE trending troughs, before the development of a large-scale episode of rift basin formation (e.g., Uliana et al., 1989; Franzese and Spalletti, 2001; Giacosa, 2020).

7.3. Tectonometamorphic and magmatic evolution

The Sierra de Calcatapul is a ~5–6 km thick by 35–40 km long Andean tectonic block bounded by NW to NNW-trending Yancamil and Sierra de Calcatapul faults to the southwest and northeast, respectively (Fig. 11). They are long-lived, sub-parallel high-angle reverse dip-slip faults plunging to the NE, inherited from the structural framework of the Paleozoic igneous-metamorphic basement (Giacosa, 2020; Giacosa et al., 2017, 2020).

After syn-rift sedimentation, the inversion of the Yancamil fault could have mastered the tectono-metamorphic D_1-M_1 evolution of the Calcatapul Formation from the Norian (c. 227 Ma). In the Puesto Yancamil area, shortening accommodated through positive inversion of inherited basement normal faults led to the formation of a folded structure accompanied by an oblique high-angle shear zone. The thin-skinned folded volcano-sedimentary pile propagated southwestward against a block of strong Yancamil Granite, acting as a buttress, inhibiting complete inversion of the Yancamil half-graben (Fig. 2). The tectonic reactivation style is localized along the granite contact, accommodating further propagation moves, forming the NNW-SSE trending shear zone and a parallel axial zone of an antiformal stack northeastward. The folded volcano-sedimentary pile decreases the frequency and increases the wavelength of its folds towards the northeast. However, the folded structure within phyllites was difficult to reconstruct owing to a lack of marker horizons/polarity markers (Fig. 6a). Kinematic indicators in both senses of shear across the fold-and-fault belt indicate re-shearing consistent with tectonic inversion.

The heterogeneous deformation is accompanied by dynamic greenschist facies (biotite grade) metamorphism, as is recorded by metamorphic mineral assemblages (Fig. 8). The metamorphic grade increases towards the buttress, reaching its maximum under amphibolite facies (sillimanite zone) within the shear zone. Temperatures of about below 500–650 °C can be inferred to the formation of the granitic mylonites, as is indicated by the advanced recrystallization of K-feldspar along the rims of porphyroclasts and sillimanite defining the mylonitic foliation (e.g., Trouw et al., 2010). The highest geothermal gradient reached along the shear zone may have contributed to combining various sources, e.g., shear heating and residual heat from the active volcanism, also involving high heat-flow derived from the upwelling of the asthenospheric mantle wedge below the rifting zone. Then, within the metamorphosed sequence, low-to high-grade solid-state crystallization and recrystallization textures predominate over the formation of typical mylonitic textures.

The structural framework of the Yancamil half-graben, dominated by tectonic inversion and accompanied by medium to high-grade dynamic metamorphism, can likely be correlated over the Uribe half-graben. However, the buttress of the NE-dipping high-angle fault/shear zone has not been identified to the southwest, and the vergence of the fold-and-fault belt is opposite concerning that of the Yancamil area (Figs. 5 and 6). Owing to meta-volcano-sedimentary blocks are entirely bounded by faults, the most likely structural geometry is a system of imbricate duplexes that branch off from a single basal fault and merge with another fault above. The roof of the belt is nowadays rubbed by Andean uplift and erosion. Assuming the same buttress with fault geometry, the NE-directed tectonic transport of imbricate duplexes can likely be the result of a NE-retrovergent duplex system of the main fault (e.g., McClay, 1995).

The intrusions of the Lipetrén Suite and equivalents taking place into already deformed-metamorphosed Calcatapul Formation indicates, on the one hand, the incomplete inversion of the Yancamil and Uribe half-grabens at the timing of emplacement, which occurred c. 215-213 Ma. On the other hand, point to the exhumation of the Calcatapul Formation was at shallower crustal levels concerning the D_1-M_1 event. Volcanic porphyritic textures, miarolitic cavities, syn-magmatic dykes, and contact metamorphism on country rocks, among others, are shallow-level magmatic features of the Lipetrén Suite (Nullo, 1978; Proserpio, 1978). Taken in conjunction with average Al-in-Hornblende geobarometric data of ~1 kb (Rapela et al., 1992), suggest an emplacement depth of around below 3 km to Lipetrén Suite, though higher pressure data of up to 3 kb translated into the depth of <11 km were reported to older Gastre granitoids (Zaffarana et al., 2014). Then, it is reasonable to assume that the Sierra de Calcatapul was at a depth less than or equal to 3 km during the Norian-Rhaetian time span.

The final exhumation of the Sierra de Calcatapul through the Yancamil fault occurred after the emplacement of Gastre-Lipetrén granitoid plutons by ~ Rhaetian. In this regard, the D_2 deformation affecting the Lipetrén Suite and its country rocks together can likely result from the late compressive effects related to tectonic inversion, which occurred within the 208-202 Ma time interval. This also indicates another significant hiatus for the central Patagonian region, including uplift and erosion to expose the cupolas of Triassic plutonic rocks shortly after its emplacement and before the effusion of overlaying volcanic rocks of the Taquetrén Formation starting in 192 Ma. This unconformity has regional distribution within the Andean Patagonian foreland, and the hiatus can be constrained between 202 and 192 Ma (Fig. 12). It was formed by widespread lithospheric extension throughout Patagonia that drove the rift basins formation where the Jurassic-Cretaceous volcano-sedimentary sequences were deposited (e.g., Giacosa, 2020 and several references therein). It is also related in space and time with the so-called "*Rioatuélica unconformity*" formed by the "*Río Atuel extensional phase*" of

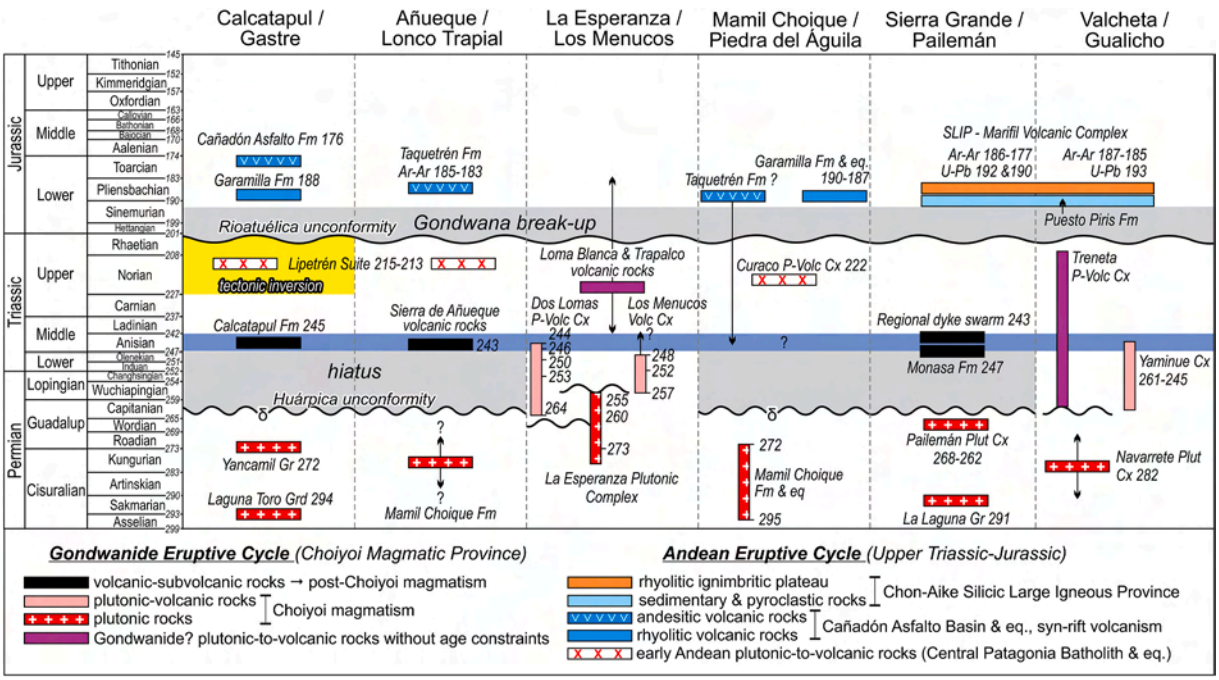

Fig. 12. Regional correlation of schematic stratigraphic sections through eastern and western parts of the North Patagonian Massif. The numbers refer to U–Pb zircon ages, except for those indicated as Ar–Ar, depicted in Ma. Fm: Formation; Gr: Granite; Grd: Granodiorite; P-Volc Cx: Plutonic-Volcanic Complex; Volc Cx: Volcanic Complex; Plut Cx: Plutonic Complex; SLIP: Silicic Large Igneous Province. Geochronological references: Grecco et al. (1994); Féraud et al. (1999); Franzese et al. (2002); von Gosen and Loske (2014); Varela et al. (2005); Pankhurst et al. (2006); Grecco and Grégori (2011); Zaffarana and Somoza (2012); Benedini and Grégori (2013); Cúneo et al. (2013); García et al. (2014); Lagorio et al. (2015); Bouhier et al. (2017); Benedini et al. (2014); Luppo et al. (2018, 2019); Martínez Dopico et al. (2017a, 2017b, 2019); Grégori et al. (2018, 2020); González et al. (2014, 2017); Chernicoff et al. (2013); Strazzere et al. (2017, 2018); Zaffarana et al. (2108), and Pavón Piveta et al. (2019).

Late Triassic-Early Jurassic age in the Andean region (e.g., Leanza, 2009).

7.4. Regional correlations

Regional correlations of the Middle Triassic post-Choiyoi magmatism of the Sierra de Calcatapul can be derived through different regions of the North Patagonian Massif, based on original stratigraphic features and U–Pb magmatic crystallization ages, which are summarized in Fig. 12. Towards the northeast of the inverted Yancamil-Uribe half-grabens, at Añueque-Lonco Trapial hills, the outcrops of a thick meso-silicic volcano-sedimentary sequence dated at 242.9 ± 2.5 Ma (Franzese et al., 2002) can be considered as the undeformed and non-metamorphosed correlative equivalent of the Calcatapul Formation. They were gathered within the overlaying Jurassic volcanic rocks assigned to the Taquetrén Formation (Nullo, 1978). Still, they must be separated from it because they belong to an older magmatic succession (Franzese et al., 2002). Such separation needs to be verified with new mappings to support its areal extent and a redefinition of its basal and top stratigraphic contacts and whether or not it is deposited in a half-graben. In the intervening time, we can refer to them informally as *"Sierra de Añueque volcanic rocks."*

In the Sierra Grande-Pailemán area, extensional tectonics related with the post-Choiyoi magmatism is evidenced by (1) the emplacement of a regional scale trachyandesitic dyke swarm dated at 243.6 ± 1.7 Ma (González et al., 2014); and (2) the effusion of andesites, andesitic basalts, trachytes, and volcanogenic agglomerates/breccias of the Monasa Formation, dated at 247.2 ± 0.46 Ma (González et al., 2017). The dikes intruded, and the volcanic pile overlays the Permian Pailemán Plutonic Complex, respectively, and in turn, they are unconformably covered by the rhyolitic ignimbritic plateau of the Jurassic Marifil Volcanic Complex (Franchi et al., 2001; González et al., 2017). Based on the petrographic, geochemical, and geochronological point of view, they are consanguineous and recorded as post-orogenic magmatism related to the extensional collapse of the Gondwanide orogen (González et al., 2017). Therefore, they can be ascribed as lateral correlative equivalents of the Calcatapul Formation (Fig. 12).

The Los Menucos Volcanic Complex (Cucchi et al., 2001) and Dos Lomas Plutonic-Volcanic Complex (Llambías and Rapela, 1984) are coeval within the main Choiyoi magmatism of the La Esperanza-Los Menucos area. They are associated with an extensional regime and consist of plutonic to sub-volcanic bodies, lava-, and pyroclastic flows controlled by ~ E-W trending normal faults in a rift-type basin (Giacosa et al., 2007). The Las Pampas Ignimbritic Rhyolite belonging to the Dos Lomas Complex (Llambías and Rapela, 1984; Llambías et al., 1984) erupted at 246 ± 2 Ma (Pankhurst et al., 2006) and an aplitic dike dated at 244.1 ± 1.6 Ma (Luppo et al., 2019) represents the youngest stages related to extensional post-Choiyoi magmatism. These ages overlap with those of the Calcatapul Formation. Moreover, both Triassic or Jurassic andesites and andesitic agglomerates of the Loma Blanca volcanic rocks overlay the Permian basement rocks and Los Menucos Volcanic Complex (Cucchi et al., 2001), suggesting either a protracted post-Choiyoi volcanic history or Jurassic syn-extensional magmatism related to normal faults (Corbella, 1973). Due to the lack of radiometric dating, the same stratigraphic uncertainties are found within the Triassic (?)-Jurassic (?) volcanic complexes from the Mamil Choique-Piedra del Aguila and Valcheta-Gualicho areas (Fig. 12).

Extensional depocenters contemporary with the post-Choiyoi Uribe and Calcatapul half-grabens and filled with volcano-sedimentary deposits are recorded along the Chilean Precordillera, Frontal Cordillera, and Principal Cordillera (inset of Fig. 1), thought their tectonic setting is still a matter of debate. It may be linked to either the extensional collapse of the Gondwanide orogen or the earliest stages of the generalized rifting process related to the opening of the back-arc Neuquén Basin. In the Principal Cordillera, the so-called *"Precuyano"* deposits (Gulisano, 1981; Carbone et al., 2011) are diachronic throughout the

area, covering the Late Triassic-Early Jurassic temporal spam. Although their isotopic constraints are still scarce, the oldest initial basin-fill volcanic deposits range mostly between 246 and 243 Ma in some depocenters (e.g., Uliana et al., 1995; Schiuma and Llambías, 2008; Spalletti et al., 2008; Suárez et al., 2008; Monti et al., 2018). For instance, the Middle Triassic-Early Jurassic Rancho de Lata Formation of the La Ramada Basin, which initiates the retroarc basin fill in the Principal Cordillera during the Andean cycle, unconformably overlies an intrusive body of the post-Choiyoi magmatism, dated at 243.5 ± 1.7 Ma (Mackaman-Lofland et al., 2019). Moreover, in the subsurface of 25 de Mayo-Medanito SE oilfields in the Neuquén Basin, five U–Pb single zircon ages on ignimbrites and tuffs yielded an average of 246 Ma for the top of the syn-rift filling, whereas a post-rift andesitic lava flow that overlaps the half-graben yielded 211 Ma (Barrionuevo et al., 2013). Or else, the U–Pb zircon ages on tuffs and acidic volcanic rocks interlayered in the sedimentary syn-rift sequence of the Rincon Blanco depocenter from the Cuyo Basin covers the range of 246–230 Ma (Barredo et al., 2012). As can be noticed, the post-Choiyoi magmatism overlaps in space and time the diachronic and isolated initiation of the rift depocenters, lava/pyroclastic flows, and ashfall deposits interlayered in the sedimentary syn-rift sequences of the Principal Cordillera and Neuquén Basin.

8. Geodynamic setting with implications

After the extensional collapse of the Late Paleozoic Gondwanide orogen implanted along the proto-Pacific continental Gondwana margin, the foreland extra-Andean central Patagonia region recorded a transitional stage with the predominance of lithospheric extension, evidenced first by the formation of local half-grabens, and then continuing with generalized regional subsidence and marine transgression cycles during the breakup of Gondwana and opening of the South Atlantic Ocean (Uliana et al., 1989; Franzese and Spalletti, 2001; Giacosa, 2020, among many others). Within this regional geodynamic setting, the widespread lithospheric extension was punctuated by the compressive effects of a tectonic phase of local character. Its distribution is limited along the southern margin of the Sierra de Calcatapul (Figs. 11 and 12). The Middle Triassic syn-extensional post-Choiyoi magmatism ceased, and the Late Triassic is a period of tectonic inversion of the Uribe and Calcatapul syn-rift wedges. In contrast, in other areas of extra-Andean Patagonia, such as the Deseado Massif (inset Fig. 1), the syn-rift deposition continues in the Late Triassic rift basins and through Early Jurassic *sag* sequences of the El Tranquilo and Roca Blanca formations (e.g., Homovc and Constantini, 2001; Jenchen and Rosenfeld, 2002; among others). Here, the syn-rift sedimentation begun during Permian with the deposition of the syn-extensional rift sequences of the La Golondrina basin, although without associated volcanism.

The tectonic inversion of the Sierra de Calcatapul within an extensional regime can likely be reconciled with the northward drifting around Pangea and displacement of South America parallel to the Late Paleozoic orogen (Vizán et al., 2017). As these authors pointed out, based on paleomagnetic constraints, NE-SW compression during the late Guadalupian-Middle Triassic period (260-240 Ma) caused counterclockwise rotational movement with differential displacements among several lithospheric domains in inner parts of Gondwana South America. These displacements induced toroidal flows in the asthenosphere, which reorganized, in turn, the geographical distribution of the rigid Gondwana domains by means of the inherited basement fault zones. This broad frame explains the local stress pattern observed in the Sierra de Calcatapul, in which NE-SW displacements could have induced the tectonic inversion through the reactivation of the Yancamil fault locally, against the buttress of the rigid Sierra del Medio granitic block (Figs. 1 and 11).

Accordingly, based on overprinting structural features revealed in the present contribution, the granitoid plutons emplacement of the Lipetrén Suite and equivalents, gathered into the Central Patagonia Batholith, was ongoing during the late-stages of the tectonic inversion. The dominant tectonic conditions during batholith emplacement were initially attributed to the NW-SE trending dextral transcurrent fault system (i.e., the so-called *"Gastre Fault System,"* Coira et al., 1975) of transcontinental scale traversing extra-Andean Patagonia (Rapela et al., 1991, 1992, see above in section 3). However, the results of microstructural and magnetic fabric analyses presented in several contributions (e.g., Franzese and Martino, 1998; Zaffarana and Somoza, 2012; Zaffarana et al., 2010, 2017, among others) mostly agree with the findings of regional tectonics of von Gosen and Loske (2014), in that the Central Patagonia Batholith spatially and temporally associated with the Gastre Fault System does not show evidence supporting the existence of a major dextral shearing active during emplacement times. Conversely, these results demonstrate that both magmatic high-temperature and solid-state low-temperature deformations occurred during the emplacement and cooling of the batholith in the Late Triassic times (Zaffarana et al., 2017; Ruiz González et al., 2020). The accommodation of the successive magmatic pulses that built the batholith (Zaffarana et al., 2012) generated heterogeneously distributed strain partitioning with deformations confined to small areas, which has different kinematics, directions, and senses (Ruiz González et al., 2020). Therefore, the temporal and spatial relationship between the emplacement of the several plutons of the Lipetrén Suite gathered into the Central Patagonian Batholith and the transcontinental dextral transcurrent tectonics along the NW-SE trending Gastre Fault System seem to be unlikely (e.g., Zaffarana et al., 2010).

Finally, a likely intra-plate tectonic setting for the compressive deformation of the Sierra de Calcatapul area can also be related to far-field stress propagated from the plate subduction margin dynamics. It predates the latest Triassic-earliest Jurassic Gondwana breakup, even considering the context of the earliest stages of the Andean magmatic arc implanted along the western margin of the supercontinent (e.g., see the compilation of Navarrete et al., 2019, which discuss the changes between the flat-slab and steep subduction angles through time).

9. Conclusions

New studies in the central extra-Andean Patagonia area allow obtaining the following conclusions:

** The Permian Yancamil Granite is the pre-rift basement on which the Middle Triassic volcano-sedimentary syn-rift sequence of the Calcatapul Formation was deposited.
** Extensional collapse of the Gondwanide Orogen formed small NNW-SSE trending half-graben basins, like those of the Yancamil and Uribe. The high-angle Yancamil normal fault-controlled the Yancamil half-graben.
** Protoliths of the Calcatapul Formation is the magmatic expression of tectonic transition from the extensional collapse of the Gondwanide Orogen and the generalized lithospheric extension ascribed to break up of Gondwana to form the proto-south Atlantic Ocean.
** U–Pb zircon ages indicate that the deposition of the volcano-sedimentary sequence occurred at 245 Ma. It is coincident with the pos-Choiyoi magmatic stage within the Patagonian setting of the Choiyoi Magmatic Province.
** A phase of positive tectonic inversion along the Yancamil fault reactivated during ~227 Ma accompanied buttressing against a rigid basement block of the Yancamil Granite during basin inversion.
** Medium to high-grade dynamic metamorphism accompanied the tectonic inversion and was higher against the buttress area.
** The tectonometamorphic event D_1-M_1 is of local distribution, circumscribed along the southern margin of the Sierra de Calcatapul area.

** The tectonic inversion outlasted the emplacement of the plutons belonging to the Lipetrén Suite into the already deformed Calcatapul Formation. The D_2 tectonic event that overprints the Lipetrén granites and the country's rocks is related to the final stages of tectonic inversion.

Declaration of competing interest

The authors declare that they have no known competing financial interests or personal relationships that could have appeared to influence the work reported in this paper.

Acknowledgments

Our sincere thanks to people from the Gastre and Yancamil areas for allowing us access to their farms and for their hospitality during our fieldwork. We warmly acknowledge the reviews by two anonymous reviewers, which improved the original manuscript significantly. We thank Dr. Sebastián Oriolo for editorial handling. This work was funded by SEGEMAR, Universidad Nacional de Río Negro (PI-UNRN-40-A-462 and PI-UNRN-40-A-622) and the Ministerio de Ciencia, Tecnología e Innovación Productiva, Agencia Nacional de Promoción Científica y Tecnológica (FONCYT, PICT-2015-0787).

Appendix A. Supplementary data

Supplementary data to this article can be found online at https://doi.org/10.1016/j.jsames.2021.103170.

References

Azcuy, C., Caminos, R., 1987. Diastrofismo. In: Archangelsky, S. (Ed.), El Sistema Carbonífero en la República Argentina. Acad. Nac. Cs. Córd., pp. 239–251.
Barredo, S., Chemale, F., Marsicano, C., Ávila, J., Ottone, E., Ramos, V., 2012. Tectono-sequence stratigraphy and U–Pb zircon ages of the rincón Blanco depocenter, northern Cuyo rift, Argentina. Gondwana Res. 21, 624–636.
Barrionuevo, M., Arnosio, M., Llambías, E., 2013. Nuevos datos geocronológicos en subsuelo y afloramientos del Grupo Choiyoi en el oeste de La Pampa: implicancias estratigráficas. Asoc. Geol. Arg. Rev. 70, 31–39.
Basei, M., Varela, R., Sato, A.M., Siga Jr., O., Llambías, E., 2002. Geocronología sobre rocas del Complejo Yaminué, Macizo Norpatagónico, Río Negro, Argentina. XV Cong. Geol. Argentino, El Calafate, Actas 3, 117–122.
Benedini, L., Grégori, D., 2013. Significance of the early jurassic garamilla Formation in the western nordpatagonian Massif. J. South Am. Earth Sci. 45, 259–277.
Benedini, L., Grégori, D., Strazzere, L., Falco, J., Dristas, J., 2014. Lower Pliensbachian caldera volcanism in high-obliquity rift systems in the western North Patagonian Massif, Argentina. J. South Am. Earth Sci. 56, 1–19.
Bouhier, V., Franchini, M., Caffe, P., Maydagán, L., et al., 2017. Petrogenesis of volcanic rocks that host the world-class Ag/Pb navidad district, North Patagonian Massif: comparison with the jurassic chon aike volcanic province of Patagonia, Argentina. J. Volcanol. Geoth. Res. 338, 101–120.
Cábana, M.C., Marchionni, D., 2011. Identificación de cuerpos máfico-ultramáficos serpentinizados a partir de imágenes ASTER en Sierras Pampeanas Orientales de Córdoba. XVIII Cong. Geol. Argentino, Neuquén, Actas electrónicas, p. 1064.
Cábana, M.C., Zaffarana, C., Orts, D., Somoza, R., 2017. Análisis espectral de datos ASTER de la región de Gastre, Chubut, Argentina. XX Cong. Geol. Argentino, San Miguel de Tucumán. Sesión Técnica 14, 9–14.
Caminos, R., Chernicoff, J., Fauqué, L., Franchi, M., 2001. Hoja geológica 4166-I, Valcheta, provincia de Río Negro. Instituto de Geología y recursos minerales, serv. Geol. Min. Argentino, Boletín 310, 1–73.
Carbone, O., Franzese, J., Limeres, M., Delpino, D., Martínez, R., 2011. El Ciclo Pre-Cuyano (Triásico Tardío-Jurásico Temprano) en la Cuenca Neuquina. In: Leanza, H., Arregui, C., Carbone, O., Danieli, J., Vallés, J. (Eds.), Geología y Recursos Naturales de la Provincia de Neuquén, Relatorio XVIII Cong, vol. 7. Geol. Arg., pp. 63–76
Coira, B., Nullo, F., Proserpio, C., Ramos, V., 1975. Tectónica de basamento de la región Occidental del Macizo Nordpatagónico (Prov. de Río Negro y Chubut) República Argentina. Asoc. Geol. Arg. Rev. 30 (3), 361–383.
Corbella, H., 1973. Basaltos nefelínicos asociados al graben del cerro Piche, Macizo Nordpatagónico, provincia de Río Negro, República Argentina. Asoc. Geol. Arg. Rev. 28 (3), 209–218.
Cucchi, R., 1993. La Formación Lipetrén en el marco del Gondwana: sector Occidental del Macizo Nordpatagónico. XII Cong. Geol. Argentino & II Cong. Explor. Hidroc., Mendoza, Actas 4, 105–122.
Cucchi, R., Busteros, A., Lema, H., Dalponte, M., Espejo, P., 2001. Hoja geológica 4169-II, los Menucos, provincia de Río Negro. Instituto de Geología y recursos minerales, serv. Geol. Min. Argentino, Boletín 265, 1–105.
Cúneo, R., Ramezani, J., Scasso, R., Pol, D., et al., 2013. High-precision U-Pb geochronology and a new chronostratigraphy for the cañadón asfalto basin, chubut, central Patagonia: implications for terrestrial faunal and floral evolution in jurassic. Gondwana Res. 24 (3), 1267–1275.
Chernicoff, C., Zappettini, E., Santos, J., McNaughton, N., Belusova, E., 2013. Combined U-Pb SHRIMP and Hf isotope study of the late paleozoic yaminué Complex, rio Negro province, Argentina: implications for the origin and evolution of the Patagonia composite terrane. Geosci. Front. 4, 37–56.
Féraud, G., Alric, V., Fornari, M., Bertrand, H., Haller, M., 1999. 40Ar/39Ar dating of the Jurassic volcanic province of Patagonia: migrating magmatism related to Gondwana breakup and subduction. Earth Planet Sci. Lett. 172 (1), 83–96.
Figari, E., Scasso, R., Cúneo, R., Escapa, I., 2015. Estratigrafía y evolución geológica de la Cuenca de Cañadón Asfalto, provincia del Chubut, Argentina. Lat. Am. J. Sedimentol. Basin Anal. 22 (2), 135–169.
Franchi, M., Ardolino, A., Remesal, M., 2001. Hoja geológica 4166 III, cona niyeu, provincia de Río Negro. Instituto de Geología y recursos minerales, serv. Geol. Min. Argentino, Boletín 262, 1–87.
Franzese, J., Martino, R., 1998. Aspectos cinemáticos y tectónicos de la zona de cizalla de Gastre en la Sierra de Calcatapul, Provincia de Chubut, Argentina. X Cong. Latinoam. Geol. & VI Cong. Nac. Geol. Econ., Buenos Aires, Actas 2, 3.
Franzese, J., Spalletti, L., 2001. Late Triassic-Early Jurassic continental extension in southwestern Gondwana: tectonic segmentation and pre breakup rifting. J. South Am. Earth Sci. 14, 257–270.
Franzese, J., Pankhurst, R., Rapela, C., Spalletti, L., et al., 2002. Nuevas evidencias geocronológicas sobre el magmatismo Gondwánico en el noroeste del Macizo Norpatagónico. XV Cong. Geol. Argentino, El Calafate, Actas 1, 144–148.
García, V., González, S.N., Tassinari, C., Sato, K., et al., 2014. Geoquímica y geocronología del Plutón La Verde, Macizo Nordpatagónico, provincia de Río Negro. XIX Cong. Geol. Argentino, Córdoba. Actas CD 373–374.
Giacosa, R., 1997. Geología y petrología de las rocas pre-cretácicas de la región de sierra Pailemán, Provincia de Río Negro. Asoc. Geol. Arg. Rev. 52 (1), 65–80.
Giacosa, R., 2020. Basement control, sedimentary basin inception and early evolution of the Mesozoic basins in the Patagonian foreland. J. South Am. Earth Sci. 97, 102407.
Giacosa, R., González, P.D., Bilmes, A., Hernando, I., 2020. Estructura y tectónica del Macizo Nordpatagónico y Precordillera Patagónica en Chubut. In: Giacosa, R. (Ed.), Geología y Recursos Naturales de la Provincia de Chubut, Relatorio del XXI Cong, vol. 1. Geol. Arg, p. 32 (in press).
Giacosa, R., Silva Nieto, D., Busteros, A., Lagorio, S., Hernando, I., 2017. Estructuras preandinas y andinas en la región Occidental del Macizo Nordpatagónico (41°-43° S). XX Cong, vol. 13. Geol. Argentino, Actas ST-, pp. 60–65.
Giacosa, R., Lema, H., Busteros, A., Zubia, M., et al., 2007. Estructura del Triásico de la región norte del Macizo Nordpatagónico (40°-41°S, 67°30'-69°45Ó), Río Negro. Asoc. Geol. Arg. Rev. 62 (3), 355–365.
Giambiagi, L., Martinez, A., 2008. Permo-Triassic oblique extension in the Potrerillos-Uspallata area, western Argentina. J. South Am. Earth Sci. 26, 252–260.
Gifkins, C., Herrmann, W., Large, R., 2005. Altered Volcanic Rocks. A Guide to Description and Interpretation. CODES Key Centre, University of Tasmania, p. 275.
González, P.D., Giacosa, R., 2020. B1. Rocas metamórficas e ígneas del Paleozoico. In: Giacosa, R., et al. (Eds.), Relatorio de la Geología y Recursos Naturales de la Provincia de Chubut. XXI Cong. Geol. Argentino, Puerto Madryn, Chubut, p. 120 (in press).
González, P.D., Sato, A.M., Naipauer, M., Varela, R., et al., 2018. Patagonia-Antarctica Early Paleozoic conjugate margins: cambrian synsedimentary silicic magmatism, U–Pb dating of K-bentonites, and related volcanogenic rocks. Gondwana Res. 63, 186–225.
González, S.N., Greco, G., González, P.D., Sato, A.M., et al., 2014. Geología, petrografía y edad U-Pb de un enjambre longitudinal NO-SE de diques del Macizo Nordpatagónico Oriental, Río Negro. Asoc. Geol. Arg. Rev. 71, 174–183.
González, S.N., Greco, G., Sato, A.M., Llambías, E., et al., 2017. Middle Triassic trachytic lava flows associated with coeval dyke swarm in the North Patagonian Massif: a postorogenic magmatism related to extensional collapse of the Gondwanide orogen. J. South Am. Earth Sci. 75, 134–143.
Greco, G., González, P.D., González, S.N., Sato, A.M., et al., 2015. Geology, structure and age of the nahuel niyeu Formation in the Aguada cecilio area, North Patagonian Massif, Argentina. J. South Am. Earth Sci. 62, 12–32.
Grecco, L., Grégori, D., 2011. Geoquímica y geocronología del Complejo Plutónico Pailemán, Comarca Nordpatagónica, Provincia De Río Negro. XIII Cong. Geol. Argentino, Neuquén, Actas CD, p. 1.
Grecco, L., Grégori, D., Rapela, C., Pankhurst, R., Labudía, C., 1994. Peraluminous granites in the Northeastern sector of the north patagonian Massif. VII Cong. Geol. Chileno, Concepción, Actas 2, 1354–1359.
Grégori, D., Saini-Eidukat, B., Benedini, L., Strazzere, L., et al., 2018. The Gondwana orogeny in northern North Patagonian Massif: evidences from the caita có granite, La seña and pangaré mylonites, Argentina. Geos. Front. Times 7 (4), 621–638.
Grégori, D., Strazzere, L., Barros, M., Benedini, L., et al., 2020. The mencué batholith: permian episodic arc-related magmatism in the western North Patagonian Massif, Argentina. Int. Geol. Rev. https://doi.org/10.1080/00206814.2019.1710865.
Gulisano, C., 1981. El ciclo Cuyano en el norte de Neuquén y sur de Mendoza. VIII Cong. Geol. Argentino, Actas 3, 579–592.
Heredia, N., Rodríguez Fernández, L.R., Gallastegui, G., Busquets, P., Colombo, F., 2002. Geological setting of the Argentine Frontal Cordillera in the flat-slab segment (30°00' to 31°30'S latitude). In: Ramos, V., McNulty, B. (Eds.), Flat Subduction in the Andes, vol. 15. J. South Am. Earth Sci., pp. 79–99
Hervé, F., Haller, M., Duhart, P., Fanning, C., 2005. SHRIMP U-Pb ages of detrital zircons from Cushamen and Esquel formations, North Patagonian Massif, Argentina: geological implications. XVI Cong. Geol. Argentino, La Plata, Actas 2, 309–314.

Hervé, F., Calderón, M., Fanning, M., Pankhurst, R., et al., 2018. The country rocks of devonian magmatism in the north patagonian Massif and chaitenia. Andean Geol. 45 (3), 301–317.
Homovc, J., Constantini, L., 2001. Hydrocarbon exploration potential within intraplate shear related depocenters: Deseado and San Julián basins, southern Argentina. Am. Assoc. Petrol. Geol. Bull. 85 (10), 1795–1816.
Hoskin, P.W.O., Schaltegger, U., 2003. The composition of zircon and igneous and metamorphic petrogenesis. In: Hanchar, J., Hoskin, P. (Eds.), Zircon. Mineralogical Society of America. Rev. Mineral. Geochem, vol. 53, pp. 27–62.
Jenchen, U., Rosenfeld, U., 2002. Continental Triassic in Argentina: response to tectonic activity. J. S. Am. Earth Sci. 15, 461–479.
Kay, S.M., Ramos, V.A., Mpodozis, C., Sruoga, P., 1989. Late paleozoic to jurassic silicic magmatism at the Gondwana margin: analogy to middle proterozoic in north America? Geology 17, 324–328.
Lagorio, S., Busteros, A., Silva Nieto, D., Giacosa, R., 2015. Nuevas edades U-Pb SHRIMP en granitoides del Batolito de la Patagonia Central, Gastre, Provincia del Chubut (República Argentina). XIV Cong. Geol. Chileno, La Serena, Actas 874–877.
Lagorio, S., Busteros, A., Silva Nieto, D., Zaffarana, C., Giacosa, R., 2020. B.7. Los granitoides pérmicos y triásicos de la región de Gastre y Sierra del Medio, suroeste del Macizo Norpatagónico. In: Giacosa, R., et al. (Eds.), Relatorio de la Geología y Recursos Naturales de la Provincia de Chubut. XXI Cong. Geol. Argentino, Puerto Madryn, Chubut, p. 56 (in press).
Leanza, H.A., 2009. Las principales discordancias del Mesozoico de la Cuenca Neuquina según observaciones de superficie. Rev. Mus. Argent. Ciencias Nat. 11, 145–184.
Lema, H., Busteros, B., Giacosa, R., Cucchi, R., 2008. Geología del Complejo Volcánico Los Menucos en el área tipo, Rio Negro. Asoc. Geol. Arg. Rev. 63, 3–13.
Lizuaín, A., Silva Nieto, D., Márquez, M., Pezzuchi, H., 2019. Hoja Geológica 4369 I, Gastre, provincia del Chubut. Instituto de Geología y Recursos Minerales, Serv. Geol. Min. Argentino, Boletín inédito, pp. 1–77.
Lesta, P., Ferello, R., Chebli, G., 1980. Chubut extraandino. In: Turner, J.C. (Ed.), Segundo Simposio de Geología Regional Argentina. Acad. Nac. Cs. Córd., pp. 1307–1387.
Luppo, T., Lopez de Luchi, M., Rapalini, A., Martínez Dopico, C., et al., 2018. Geochronologic evidence of a large magmatic province in northern Patagonia encompassing the Permian-Triassic boundary. J. S. Am. Earth Sci. 82, 346–355.
Luppo, T., Martínez Dopico, C., Rapalini, A., López de Luchi, M., et al., 2019. Paleomagnetism of Permo–Triassic volcanic units in northern Patagonia: are we tracking the final stages of collision of Patagonia? Int. J. Earth Sci. 108 (2), 621–647.
Ludwig, K., 2003. Isoplot/Ex, v.3. A Geochronological Toolkit for Microsoft Excel, vol. 4. Berkeley Geochronology Center, Special Publication, p. 71.
Llambías, E., Rapela, C., 1984. Geología de los complejos eruptivos del Paleozoico superior de La Esperanza, provincia de Río Negro. Asoc. Geol. Arg. Rev. 39, 220–243.
Llambías, E.J., Sato, A.M., 1995. El batolito de Colangüil: transición entre orogénesis y anorogénesis. Asoc. Geol. Arg, Rev. 50 (1–4), 111–131.
Llambías, E., Sato, A.M., 2011. Ciclo Gondwánico: la Provincia Magmática Choiyoi en Neuquén. In: Leanza, H., Arregui, C., Carbone, O., Danieli, J., Vallés, J. (Eds.), Geología y Recursos Naturales de la Provincia de Neuquén, Relatorio XVIII Cong, vol. 6. Geol. Arg., pp. 53–62
Llambías, E., Caminos, R., Rapela, C., 1984. Las plutonitas y vulcanitas del Ciclo Eruptivo Gondwánico. In: Ramos, V. (Ed.), Geología y Recursos Naturales de la Provincia de Río Negro, Relatorio IX Cong, vols. I-4. Geol. Arg., pp. 85–117
Llambías, E., Varela, R., Sato, A.M., 2002. Deformación y metamorfismo neopaleozoico en Yaminué, Macizo Norpatagónico (40°50'S, 67°40'O): su relación con la Fase Orogénica San Rafael y el arco de los Gondwánides. XV Cong. Geol. Argentino, El Calafate, Actas 3, 123–128.
Mackaman-Lofland, Ch, Horton, B., Fuentes, F., Constenius, K., Stockli, D., 2019. Mesozoic to Cenozoic retroarc basin evolution during changes in tectonic regime, southern Central Andes (31-33°S): insights from zircon U-Pb geochronology. J. S. Am. Earth Sci. 89, 299–318.
Martínez Dopico, C., Tohver, E., López de Luchi, M., Rapalini, A., et al., 2017a. Jurassic cooling ages in Paleozoic to early Mesozoic granitoids of northeastern Patagonia: 40Ar/39Ar, 40K/40Ar mica and U-Pb zircon evidence. Int. J. Earth Sci. 106 (7), 2343–2357.
Martínez Dopico, C., López de Luchi, M., Rapalini, A., Wemmer, K., et al., 2017b. Emplacement and temporal constraints of the Gondwanan intrusive complexes of Northern Patagonia: La Esperanza plutono-volcanic case. Tectonophysics 712–713, 249–269.
Martínez Dopico, C., López de Luchi, M., Rapalini, A., Fanning, M., et al., 2019. Geochemistry and geochronology of the shallow-level La Esperanza magmatic system (Permian-Triassic), northern Patagonia. J. S. Am. Earth Sci. 96, 102347.
McClay, K.R., 1995. Geometries and kinematics of inverted fault systems. In: Buchanan, J., Buchanan, P. (Eds.), Basin Inversión, vol. 88. Geological Society London, Special Publication, pp. 97–118.
McPhie, J., Doyle, M., Allen, R., 1993. Volcanic Textures. A Guide to the Interpretation of Textures in Volcanic Rocks. CODES Key Centre. University of Tasmania, p. 198.
Möller, A., Kennedy, A., 2006. Extremely high Th/U in metamorphic zircon: in situ dating of the Labwor Hills granulites. Goldschmidt Conference Abstracts. Geochem. Cosmochim. Acta 70 (18). https://doi.org/10.1016/j.gca.2006.06.855. A425-A425.
Monti, M., Sato, A.M., Franzese, J., 2018. Edad del rifting triásico en la cuenca de Puesto Viejo (U-Pb 243,9 ± 2 Ma), San Rafael, provincia de Mendoza. XVI Reu. Arg. Sedimentología, Roca, T-S6, p. 81.
Murphy, M., Salvador, A., 2002. International stratigraphic guide-an abridged version. International subcommission on stratigraphic classification of IUGS. International Commission on Stratigraphy. Episodes 22 (4), 255–272.
Navarrete, C., Gianni, G., Encinas, A., Márquez, M., et al., 2019. Triassic to Middle Jurassic geodynamic evolution of southwestern Gondwana: from a large flat-slab to mantle plume suction in a rollback subduction setting. Earth Sci. Rev. 194, 125–159.
Nullo, F., 1978. Descripción Geológica de la Hoja 41d, Lipetrén, Provincia de Río Negro, 158. Ministerio de Economía, Secretaría de Estado de Minería, Boletín, pp. 1–88.
Nullo, F., Proserpio, C., 1975. La Formación Taquetrén en Cañadón del Zaino (Chubut) y sus relaciones estratigráficas en el ámbito de la Patagonia, de acuerdo a la flora, República Argentina. Asoc. Geol. Arg. Rev. 30 (2), 133–150.
Pankhurst, R., Rapela, C., Fanning, C., et al., 2006. Gondwanide continental collision and the origin of Patagonia. Earth Sci. Rev. 76, 235–257.
Pankhurst, R., Rapela, C., López de Luchi, M., Rapalini, A., et al., 2014. The Gondwana connections of northern Patagonia. J. Geol. Soc. Lond. 171, 313–328.
Pavón Pivetta, C., Grégori, D., Benedini, L., Garrido, M., et al., 2019. Contrasting tectonic settings in northern chon aike igneous province of Patagonia: subduction and mantle plume-related volcanism in the Marifil formation. Int. Geol. Rev. https://doi.org/10.1080/00206814.2019.1669227.
Pezzutti, N., Busteros, A., 1975. Estudio petrográfico de rocas procedentes de la Hoja 42d, Gastre, Provincia del Chubut. Ministerio de Economía, Secretaría de Estado de Minería. Informe Inédito, Buenos Aires, p. 18.
Proserpio, C.A., 1978. Descripción Geológica de la Hoja 42d, Gastre, Provincia del Chubut, vol. 159. Ministerio de Economía, Secretaría de Estado de Minería, Boletín, pp. 1–75.
Ramos, V.A., 1988. The tectonics of the Central Andes: 30°-33°S latitude. In: Clark, S., Burchfield, D. (Eds.), Processes in Continental Lithospheric Deformation, vol. 218. Geological Society of America, Special Papers, Boulder, pp. 31–54.
Ramos, V.A., 2008. Patagonia: a Paleozoic continent adrift? J. S. Am. Earth Sci. 26, 235–251.
Rapela, C., Llambías, E., 1985. Evolución magmática y relaciones regionales de los complejos eruptivos de La Esperanza, provincia de Rio Negro. Asoc. Geol. Argent. Rev. 40, 4–25.
Rapela, C., Dias, G., Franzese, J., Alonso, G., Benvenuto, A., 1991. El batolito de la Patagonia central: evidencias de un magmatismo triásico-jurásico asociado a fallas transcurrentes. Rev. Geol. Chile 18 (2), 121–138.
Rapela, C., Pankhurst, R., Harrison, S., 1992. Triassic "Gondwana" granites of the Gastre district, North Patagonian Massif. Trans. R. Soc. Edinb. Earth Sci. 83, 291–304.
Rapela, C., Pankhurst, R., Fanning, C., Hervé, F., 2005. Pacific subduction coeval with the Karoo mantle plume: the Early Jurassic Subcordilleran belt of northwestern Patagonia. In: Vaughan, A., Leat, P., Pankhurst, R. (Eds.), Terrane Processes at the Margins of Gondwana, vol. 246. Geol. Soc. London, Special Publication, pp. 217–239.
Ravazzoli, I., Sesana, F., 1977. Descripción Geológica de la Hoja 41c, Río Chico, Provincia de Río Negro, vol. 148. Ministerio de Economía, Secretaría de Estado de Minería, Boletín, pp. 1–82.
Ruiz González, V., Puigdomenech, C., Zaffarana, C., Vizán, H., Somoza, R., 2020. Paleomagnetic evidence of the brittle deformation of the central patagonian batholith at Gastre area (chubut province, Argentina). J. S. Am. Earth Sci. 98, 102442.
Sato, K., Siga Jr., O., da Silva, J., McReath, I., et al., 2009. In Situ Isotopic Analyses of U and Pb in zircon by remotely operated SHRIMP II, and Hf by LA-ICP-MS: an example of dating and genetic evolution of zircon by 176Hf/177Hf from the Ita Quarry in the Atuba Complex, SE Brazil. Rev. Inst. Geociências 9 (3), 61–69.
Sato, K., Basei, M., Ferreira, C., Vlach, S., et al., 2010. In Situ U-Th-Pb Isotopic Analyses by Excimer Laser ablation/ICP–MS on Brazilian Xenotime Megacrystal: First U-Pb Results at CPGeo-IG-USP. 7th South American Symposium on Isotope Geology. Abstracts in CD, Brasilia, pp. 349–352.
Sato, A.M., Llambías, E., Basei, M., Castro, C., 2015. Three stages in the Late Paleozoic to Triassic magmatism of southwestern Gondwana, and the relationships with the volcanogenic events in coeval basins. J. S. Am. Earth Sci. 63, 48–69.
Schiuma, M., Llambías, E., 2008. New ages and chemical analysis on Lower Jurassic volcanism close to the Dorsal de Huincul. Neuquén. Asoc. Geol. Arg. Rev. 63, 644–652.
Spalletti, L., Fanning, C., Rapela, C., 2008. Dating the triassic continental rift in the southern Andes: the potrerillos formation, Cuyo Basin, Argentina. Geol. Acta 6, 267–283.
Stipanicic, P., Linares, E., 1969. Edades radimétricas determinadas para la República Argentina y su significado geológico. Bol. Acad. Nac. Cs. Córd. 47 (1), 51–96.
Stipanicic, P., Rodrigo, F., Baulies, D., Martínez, C., 1968. Las formaciones pre-senonianas en el denominado "Macizo Nordpatagónico" y regiones adyacentes. Asoc. Geol. Arg. Rev. 23 (2), 67–98.
Strazzere, L., Grégori, D., Benedini, L., Marcos, P., et al., 2017. Edad y petrografía del complejo volcánico Marifil en la Sierra de Pailemán, Comarca Nordpatagónica, Rio Negro, Argentina. XX Cong. Geol. Argentino, Tucumán, Actas CD ST-8, p. 2.
Strazzere, L., Grégori, D., Benedini, L., Marcos, P., et al., 2018. The puesto piris formation: evidence of basin-development in the north patagonian Massif during crustal extension associated with Gondwana breakup. Geosc. Front. 10 (1), 299–314.
Suárez, M., de la Cruz, R., Fanning, M., Etchart, H., 2008. Carboniferous, Permian and Toarcian magmatism in Cordillera del Viento, Neuquén, Argentina: first U-Pb SHRIMP dates and tectonic implications. XVII Cong. Geol. Argentino, S.S. Jujuy. Acta 3, 906–907.
Timms, N., Kinny, P., Reddy, S., 2006. Enhanced diffusion of Uranium and Thorium linked to crystal plasticity in zircon. Geochem. Trans. 7, 10. https://doi.org/10.1186/1467-4866-7-10.
Trouw, R., Passchier, K., Wiersma, D., 2010. Atlas of Mylonites and Related Microstructures. Springer-Verlag Berlin Heidelberg, p. 322p.
Uliana, M., Biddle, K., Cerdán, J., 1989. Mesozoic extension and the formation of Argentina sedimentary basins. In: Tankard, A., Balkwill, H. (Eds.), Extensional

Tectonics and Stratigraphy of the North Atlantic Margin, vol. 46. Am. Assoc. Petrol. Geol. Memoir, pp. 599–613.
Uliana, M., Arteaga, M., Legarreta, L., Cerdán, J., et al., 1995. Inversion structures and hydrocarbon occurrence in Argentina. In: Buchanan, J., Buchanan, P.G. (Eds.), Basin Inversion, vol. 88. The Geological Society London, Special Publications, pp. 211–233.
Varela, R., Basei, M., Cingolani, C., Siga Jr., O., Passarelli, C., 2005. El basamento cristalino de los Andes norpatagónicos en Argentina: geocronología e interpretación tectónica. Rev. Geol. Chile 32 (2), 167–187.
Varela, R., Basei, M., González, P.D., Sato, A.M., Sato, K., 2008. Granitoides Famatinianos y Gondwánicos en Sierra Grande. Nuevas edades radiométricas método U-Pb. XVII Cong. Geol. Argentino, Jujuy, Actas, pp. 914–915.
Vizán, H., Prezzi, C., Geuna, S., Japas, S., et al., 2017. Paleotethys slab pull, self-lubricated weak lithospheric zones, poloidal and toroidal plate motions, and Gondwana tectonics. Geosphere 13 (5), 1541–1554.
Volkheimer, W., 1965. Bosquejo geológico del noroeste del Chubut extra-andino (zona Gastre-Gualjaina). Asoc. Geol. Arg. Rev. 20 (3), 326–350.
Volkheimer, W., 1973. Observaciones geológicas en el área de Ingeniero Jacobacci y adyacencias (Provincia de Río Negro). Asoc. Geol. Arg. Rev. 28 (1), 13–36.
Volkheimer, W., Lage, J., 1981. Descripción Geológica de la Hoja 42c, Cerro Mirador, Provincia del Chubut, vol. 181. Ministerio de Economía, Secretaría de Estado de Minería, Boletín, pp. 1–71.
von Gosen, W., 2002. Polyphase structural evolution in the northeastern segment of the North Patagonian Massif (southern Argentina). J. South Am. Earth Sci. 15, 591–623.
von Gosen, W., 2003. Thrust tectonics in the north patagonian Massif (Argentina): implications for a patagonian plate. Tectonics 22, 1005.
von Gosen, W., 2009. Stages of late palaeozoic deformation and intrusive activity in the western part of the North Patagonian Massif (southern Argentina) and their geotectonic implications. Geol. Mag. 146, 48–71.
von Gosen, W., Loske, W., 2014. Tectonic history of the Calcatapul Formation, chubut province, Argentina, and the "Gastre Fault system". J. S. Am. Earth Sci. 18, 73–88.
Zaffarana, C., Somoza, R., 2012. Paleomagnetism and 40Ar/39Ar dating from Lower Jurassic rocks in Gastre, central Patagonia: further data to explore tectonomagmatic events associated with the breakup of Gondwana. J. Geol. Soc. (Lond.) 169, 371–379.
Zaffarana, C., López de Luchi, M., Somoza, R., Mercader, R., et al., 2010. Anisotropy of magnetic susceptibility study in two classical localities of the Gastre Fault system, central Patagonia. J. S. Am. Earth Sci. 30, 151–166.
Zaffarana, C., Somoza, R., López de Luchi, M., 2014. The late triassic central patagonian batholith: magma hybridization, 40Ar/39Ar ages and thermobarometry. J. S. Am. Earth Sci. 55, 94–122.
Zaffarana, C., Somoza, R., Orts, D.L., Mercader, R., et al., 2017. Internal structure of the central patagonian batholith at Gastre. Geosphere 13 (6), 1973–1992.
Zaffarana, C., Gallastegui, G., Lagorio, S., Poma, S., et al., 2018. Geochemical signature and reservoir conditions of early jurassic calc-alkaline volcanic rocks from Lonco Trapial Formation, central Patagonia. J. S. Am. Earth Sci. 88, 415–445.